USE OF COATED ELECTRODE IN MICROWAVE-INDUCED PLASMA-IN-LIQUID PROCESS TO SYNTHESIZE METAL NANOPARTICLES

David Čempel

Graduate School of Engineering

Division of Materials Science and Engineering

Hokkaido University

This dissertation is submitted for the degree of Doctor of Philosophy

March 2018

SUMMARY

More than free decades ago Nanotechnology replaced microtechnology at the peak of scientific interest, and stays there still nowadays. Nanotechnology became in many understandings the technology of the future with wide impact on the technological development. Nanoparticles (NPs) are in immerse interest of scientific community, because they are not subjects of classical physics rules and follow quantum mechanical rules instead. NPs became very quickly part of our daily lives, from antibacterial detergents through semiconductor materials in everyday used electronic devices to their utilization in medicine.

This study aims at improving understanding of the formation of the metallic and bimetallic NPs using microwave induced plasma in liquid process (MWPLP). This method brings new opportunities for the “greener” synthesis of the NPs. It provides same or better results than conventional methods with simple process, high purity, and lower impact on the environment due to avoiding the use of toxic solvents and reducing agents. The synthesis is using microwave generated non-equilibrium plasma in water at reduced pressure to thermally decompose water molecules and provide various reactive chemical species (e.g., electrons, hydrogen radicals, hydroxyl radicals, and oxygen radicals). Produced chemical species, especially hydrogen radicals, can then reduce metallic ions. Composition and size of the NPs can be controlled by adjusting the conditions of the synthesis process. This dissertation discusses synthesis of metallic NPs using MWPLP method and focuses on challenges associated with plasma in liquid process.

Toxicity, and very costly and troublesome purification are one of the challenges associated with preparation of metallic NPs. In order to avoid these challenges,

plasma in liquid process became a hot topic for synthesis of the metallic NPs, however the use of conventional electrodes in this process brings new problems related to contamination of synthesized particles by electrode materials. My study proposed use of ceramic coated yttrium oxide (Y_2O_3) electrode which has higher elusion and erosion rate than conventional electrodes, and also exhibits enhanced electric field strength, to synthesize pure metallic NPs.

Gold (Au) NPs are one of the most studied metallic NPs and they have been used in numerous applications from jewelry to advanced technology and medicine. In my study about Au NPs, the time-dependent formation and growth of Au NPs during MWPLP was investigated together with the effect of the solution pH on Au NPs formation. We were able to obtain highly pure Au NPs with bimodal size distribution for pH in range of 3.5 – 12.0. The fraction of small sized Au NPs becomes significant at pH 6.0 and 12.0 while that of big sized Au NPs is dominant at pH 3. This change in the size distribution of Au NPs was governed by different reduction rate of gold ions at different pH.

Another metallic NPs, silver (Ag) NPs are widely used for their physical properties, biocompatibility, and low cost. These NPs need to be protected to prevent aggregation caused by their high surface energy. The influence of different precursors and the capping ability of L-arginine as a stabilizing agent on the size and uniformity of the obtained Ag NPs in MWPLP was investigated. We chose L-arginine, one of the essential amino acids, as a protecting agent for Ag NPs' synthesis, because of its biocompatibility and non-toxicity. As a result, strong dependence of NPs' uniformity on the chosen precursor (silver diamine complex in our case) was observed as well as the influence of L-arginine on the particles

growth phase. Using silver diamine as a precursor for Ag NPs synthesis can protect particles from secondary nucleation step and bimodal size distribution due to its higher reactivity in comparison with silver nitrate. The L-arginine as a capping ligand can well cap Ag NPs and has strong influence on their size. Use of L-arginine and silver diamine complex has been demonstrated as a powerful tool to produce highly uniform small sized Ag NPs of 5 nm.

Bimetallic NPs are composed of two different metal elements and show enhanced optical, catalytic, photocatalytic or electronic properties in comparison with those of monometallic NPs. The structure of bimetallic nanoparticles differs from alloy, intermetallic compound, cluster-in-cluster to core–shell structures. The structure is dependent on the relative strengths of metal-metal bond, relative atomic sizes, and also on preparation method. Au-Ag alloy bimetallic NPs have been intensively investigated due to their tunable plasmonic applications, catalysis and biosensing. In the last part of this thesis, Au-Ag alloy NPs were prepared by MWPLP without any protecting or reducing agents. Tunable composition of the finally produced NPs was achieved by varying the initial ratio of the metal precursors. XRD and XRF results further confirmed tunable composition of the Au-Ag NPs. STEM-EDS confirmed homogeneous distribution of Au and Ag over particles.

Studies in this doctoral thesis bring different approaches to metallic NPs synthesis, especially to the “green” synthesis. Preparation of highly pure metallic and bimetallic NPs, controlling their composition, and understanding of their formation during microwave plasma in liquid process can help with the progress in nanotechnology field.

Key words: Microwave plasma in liquid process, Gold nanoparticles, Silver nanoparticles, Gold-silver alloy nanoparticles

ACKNOWLEDGEMENTS

I'd like to thank Mai Thanh Nguyen for her vigorous help, and professor Tetsu Yonezawa for the opportunity to study in his laboratory and sharing his knowledge.

This work is partially supported from Hokkaido University and Japanese Government.

And at last, but not least, I'd like to thank to all the friends who have helped me during my stay in Sapporo.

LIST OF ABBREVIATIONS

Ag NPs	……..……. Silver nanoparticles
Au NPs	……..... Gold nanoparticles
EDX	……....……... Energy-dispersive X-ray spectroscopy
FT-IR	……..…….. Fourier-transform infrared spectroscopy
ICP-OES	……..….. Inductively coupled plasma atomic emission spectroscopy
L-arg	……. L-arginine
MWPLP	……. Microwave-induced plasma in liquid process
NPs	…….. Nanoparticles
PLP	……. Plasma in liquid process
SAED	……..…….. Selected area diffraction
STEM	……..…….. Scanning transmission electron microscopy
TEM	……..……. Transmission electron microscopy
TG-DTA	……..... Thermal gravimetric analysis
XRD	……... X-ray diffraction

CONTENTS

LIST OF FIGURES

1 INTRODUCTION

1.1 Nanoparticles

In the last three decades, the trend of the research in modern science has been focused on the structures with futures controlled in nanometer level. This include area of research such as engineering, physics, chemistry, materials science and molecular biology. Such materials with sizes bellow 100 nanometers show very

different characteristics compared to their bulk or micro-sized counterparts. A nanoparticle can be defined as a microscopic particle with at least one dimension less than 100 nanometers. Due to this property, surface to volume ratio increase drastically, therefore size-dependent properties can be observed, i.e. surface plasmon resonance, superparamagnetism, possible appearance of quantum effects, etc. Properties of NPs changes with increasing percentage of atoms on their surface. These particles exhibit numerous unique catalytic, optical and electronic properties. The immense interested in past decades has been given to the tailoring of their size, shape and composition to obtain variations of their properties.

Metallic and metallic alloy NPs have been used as catalysts[1], microelectronics materials[2-3], optoelectronics materials[4-7], magnetic materials[8,9], fuel cells[10] etc., and have been heavily utilized in biomedical science and engineering. Well sized controlled gold and silver nanoparticles modified by various chemical functional groups have wide range of applications such in biotechnology, target drug delivery, as vehicles for gene and drug delivery, cancer treatment and diagnostic imaging.[11-14] Bimetallic Au/Ag nanoparticles are extensively investigated for their use in catalysis, biosensing and applications in plasmonics.[15-21] Tunable properties

between the value of pure Au and Ag, as well as their internal structure (core-shell, alloy), determine their applications.

1.2 Nanoparticle synthesis methods

Nanoparticle synthesis is a method for creating nanoparticles. Nanoparticles can be prepared in “top-down” (physical) methods by subdivision of bulk metals or synthesized by ‘bottom-up’ (chemical) methods which consist of growth of particles from metal atoms obtained from molecular or ionic precursors (Figure 1.1).[22] Another classification for these methods can be dry (physical) and wet (chemical) method. These processes can produce particles from different materials with various size, shape and properties. The bottom-up method is considered to be more useful for preparation of small sized uniform nanoparticles. There are several aspects important during nanoparticles’ synthesis, i.e. energy efficiency and cost of the synthesis, industrial application, and one of the biggest concerns lately is about toxicity and environmental effect of the synthesis. We can say, that simple synthesis processes with low cost and environmental effect are preferable by other methods. Ligands and solvent-soluble polymers are often used as a stabilizer of metallic nanoparticles. These stabilizing agents can control reduction of the metal ions as well as aggregation of metal atoms, and therefore can influence particles’ size and size distribution. However, it was proved that nanoparticles can by

synthesized without any stabilizing agent as well. In the past several decades many groups were focusing on preparation of various monometallic nanoparticles (e.g. Au, Ag, Cu, Pd, Pt) and bimetallic nanoparticles (e.g. Au/Ag, Au/Pd, Au/Cu, Ag/Cu, Au/Ni).

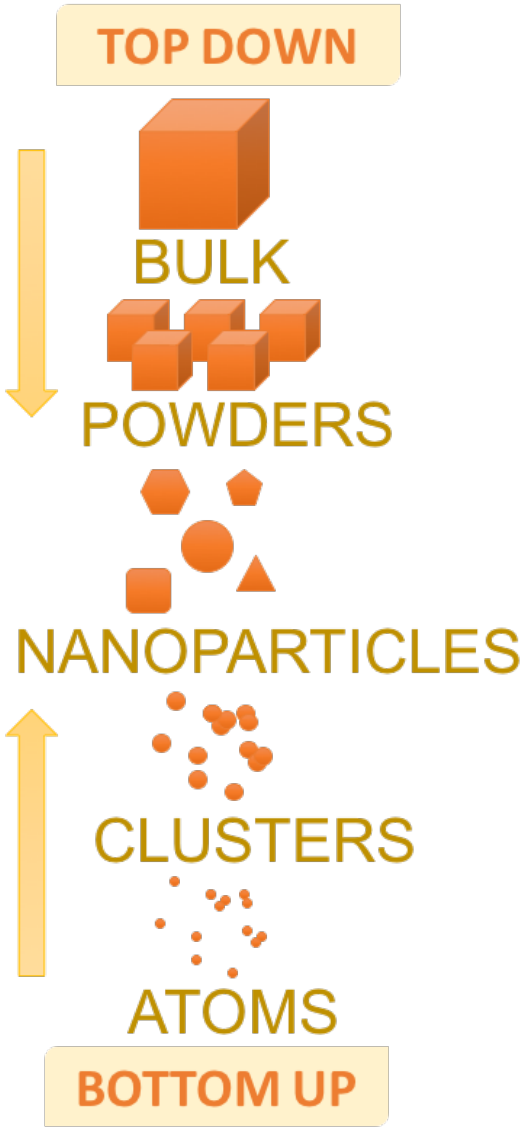

Figure 1.1 Schematic illustration of methods for preparation of nanoparticles.

Bottom-up methods

Bottom-up processes are those where the synthesis of NPs starts from single atoms. NPs are built up from the bottom: atom by atom, molecule by molecule, cluster by cluster. All the processes included in this group rely on the availability of appropriate “metal-organic” molecules, metal salts or complexes as precursors. There are several methods included in this bottom-up approach such as chemical reduction[25,26], sol-gel processing[23,24], chemical vapor deposition (CVD)[27,28], laser pyrolysis[29], and plasma processes[30-37].

1.3 Plasma

Plasma is one of four states of matter, other states include solid, liquid and gas (Figure 1.2). Unlike all the other states of matter, plasma doesn’t exist on the Earth under normal conditions. It’s interesting to realize that more than 99% of all the substances in the Universe exists in form of plasma.

Plasma is a state in which an ionized gaseous substance becomes highly electrically conductive, to the point where electric and magnetic fields dominate the behavior of the matter.[38] Term “ionized” refers to the presence of one or more free electrons, which are not bound to an atom or molecule.[39] The degree of ionization (ratio of charged over uncharged particles) can be quite small. Due to the mobile

electric charges (free electrons), a plasma is electrically conductive. It can be created artificially by heating neutral gases or by exposing the gas to the strong electromagnetic field. It contains an equal number of positive ions and negative electrons (sometimes negative ions), it also consists of neutral, metastable, excited atoms or molecules, reactive radicals and emits ultraviolet (UV) light and strong electric field.

It can be divided into thermal (equilibrium) plasmas, where thermal energy (temperature) of the ions and electrons is the same (in equilibrium), they have temperatures over 4000K, and nonthermal (nonequilibrium) plasmas where the temperature of the electrons is significantly higher than the temperature of the elements. These plasmas have temperatures below 1000K.

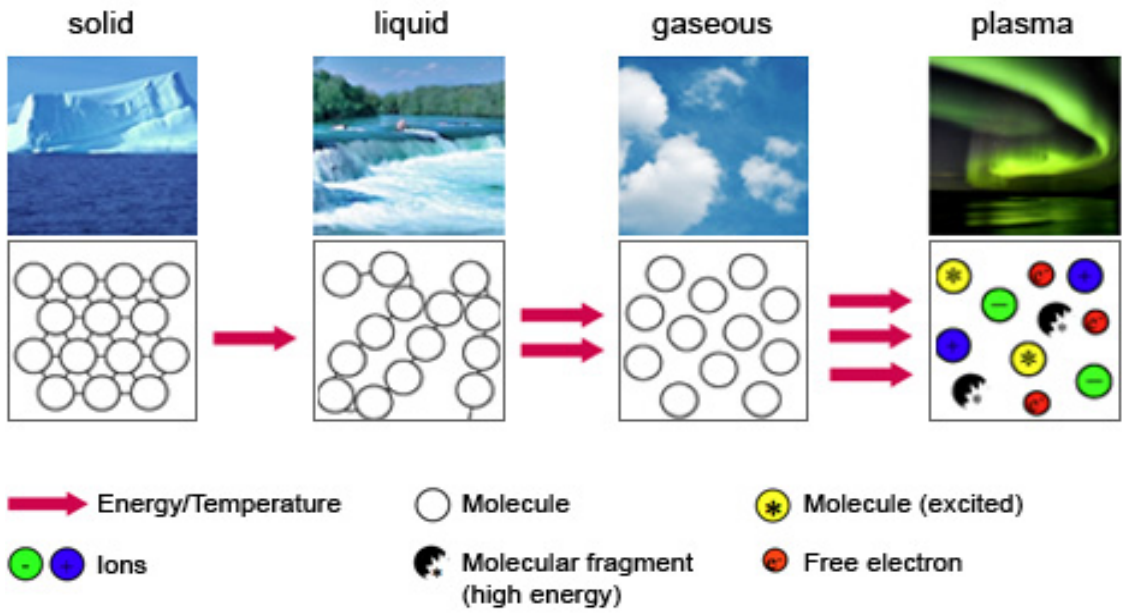

Figure 1.2 Transition of states of matter.[40]

1.4 Plasma in nanoparticle synthesis

Over the past few decades, artificially created plasmas play an important role in the NP synthesis and the field is developing rapidly. Plasma in NP synthesis can be divided into three groups in dependence on the pressure-temperature relationship: solid phase plasma, gas phase plasma and liquid phase plasma (Figure 1.3).[41] These groups can be than divided into several other subgroups. This work will mainly focus on the plasma generated in liquid since it's still relatively unknown, even with the progress in this field in the last decade. Gas-phase plasma is briefly introduced below since it's liquid plasmas' predecessor and shares some of its characteristics.

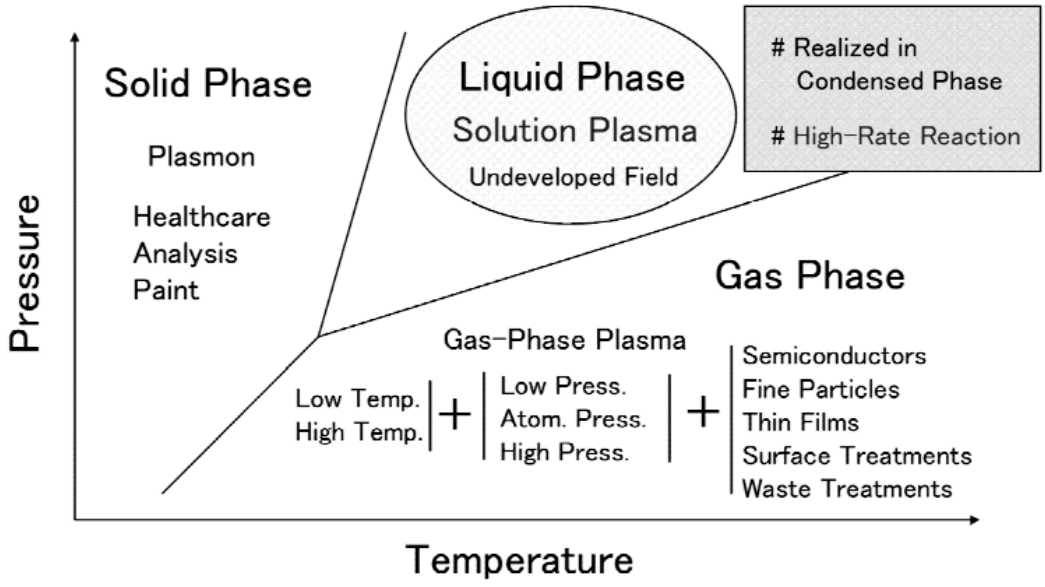

Figure 1.3 Three categories of plasma corresponding to the pressure-temperature relationship of three phases.[41]

1.4.1 Gas-phase plasma

Gas-phase plasma is used in widely used in industry, such as electronic device manufacturing processes (plasma etching, sputtering, plasma-enhanced chemical vapor deposition, etc.), hard coating processes (ion plating, sputtering, etc.), and surface treatment processes (sputtering, plasma etching, etc.).[41] Gas-phase plasma can be divided into a low and high temperature plasma and low, high and atmospheric pressure plasma. Different sub-division for this phase can be based on plasma source, i.e. alternating current (AC), direct DC current, radio frequency (RF) or microwave source.

High-temperature plasmas are the oldest and most common plasmas working at atmospheric pressure. The energy distribution in these plasmas are usually close to thermal equilibrium. Typical gas-phase plasma setup using AC or DC current is shown in Figure 1.4. This type of plasma mainly produces nanoparticles with bigger NPs' size and broad size distribution (example is showed in Figure 1.5) and in some cases, it can lead to the formation of particle clusters.[42]

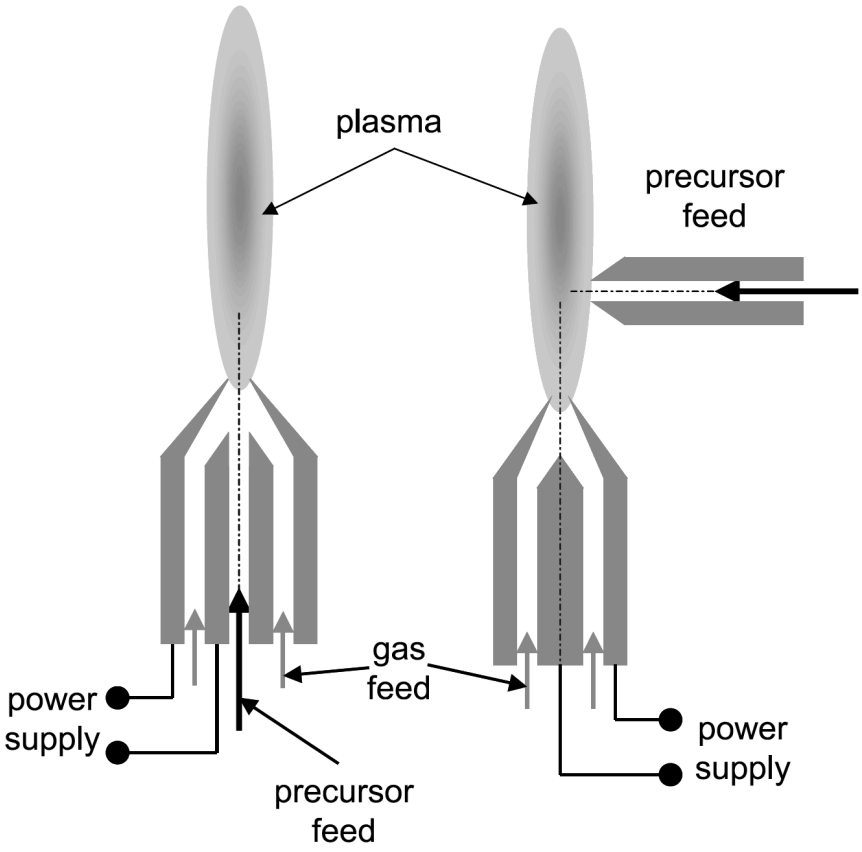

Figure 1.4 Two basic types of plasma burners for nanopowder production, differing in the way of precursor feeding (axial feed on the left and feeding from the side on the right. Both can use powder or liquid precrsors.[42]

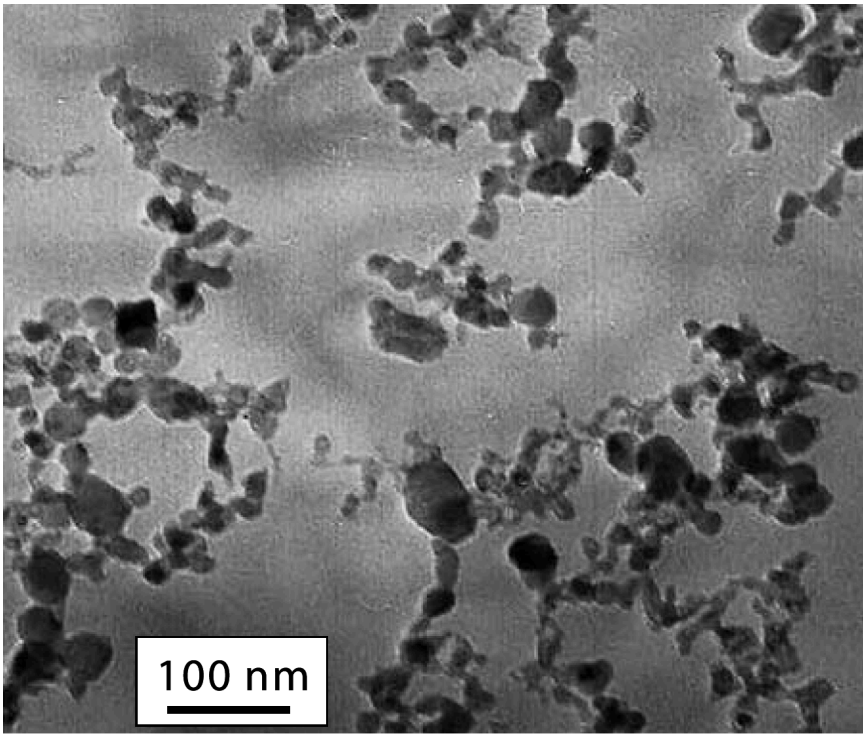

Figure 1.5 TEM image of synthesized nanocrystalline AlN (aluminum nitride). [49]

Low-temperature plasmas are always connected to the systems with reduced pressure. They have temperatures below 1000K. In this type of plasma power is supplied by either radio frequency (RF) or microwaves. Particles obtained by gas-phase low discharge plasma have narrow size distribution. Typical nanoparticles obtained by RF system (Figure 1.6) and microwave system (Figure 1.7).

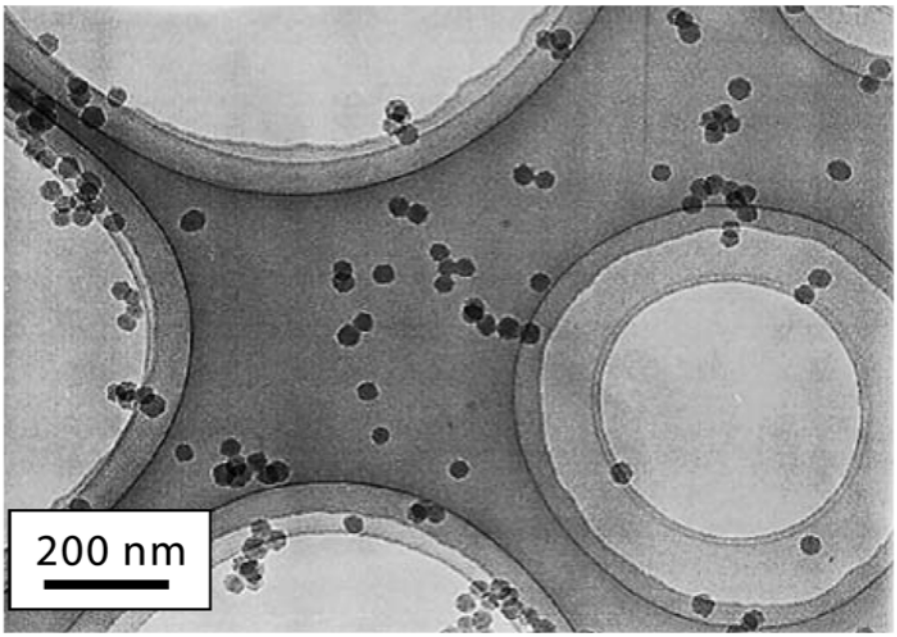

Figure 1.6 TEM of FePt NPs obtained in RF gas-phase system.[42]

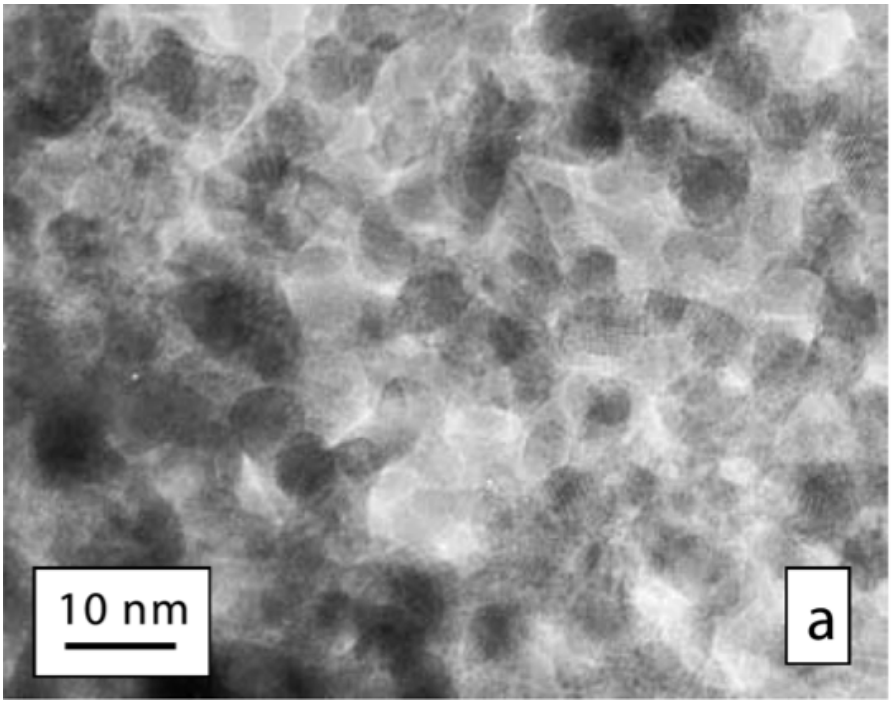

Figure 1.7 TEM of zirconia powders obtained in gas-phase microwave plasma process.[42]

1.4.2 Liquid-phase plasma

Plasma generated in liquid is a versatile process with high performance for many applications such as water purification[43], sterilization[44,45], and most importantly nanoparticles synthesis.[31,36,37,41,46-48] Plasma in liquid is a non-thermal (nonequilibrium) plasma where the plasma generation in liquid can be divided into:

(i) Gas discharge between an electrode and the electrolyte surface (Figure 1.8 a)

(ii) Direct discharge between 2 electrodes (Figure 1.8 b)

(iii) Contact discharge between an electrode and the surface of surrounding electrolyte (Figure 1.8 c)

(iv) Radio frequency (RF) (Figure 1.8 d) and microwave (MW) generation

regarding to G. Saito et al.[50] This work is focusing on the iv) group, mainly MW generated plasma in liquid.

Another dividing of plasma in liquid can be in to plasma in the bubble or small vapor channel plasma (Figure 1.9).[52] In the plasma in bubble process, bubbles consist of water vapor created by joule heating and electrolysis of water. The bubble plasma usually propagates along the plasma–liquid surface or across the bubble without contacting the liquid surface depending on the dielectric constants

of the bubble gas and liquid. The reactive species generated in the bubbles can diffuse across the plasma-liquid interface and will enter the liquid when the bubbles are broken, this is a big advantage compared to plasma over liquid system. The streamer plasma in water is generated by a decrease of the liquid density around the electrode by electric field enhancement under a high overvoltage, or direct electron collision induced liquid water ionization under an ultrahigh local electric field. The streamer plasma takes on the form of multi-branched channels.[52] The dominant active species produced by these methods are O, H, and OH radicals as well as atomic O and atomic H. Because both electrodes are immersed in the liquid, the finally produced NPs might be contaminated by the electrodes' material. Therefore, the electrode materials and solution constituents must be carefully selected in order to decrease potential impurities as much as possible.[52]

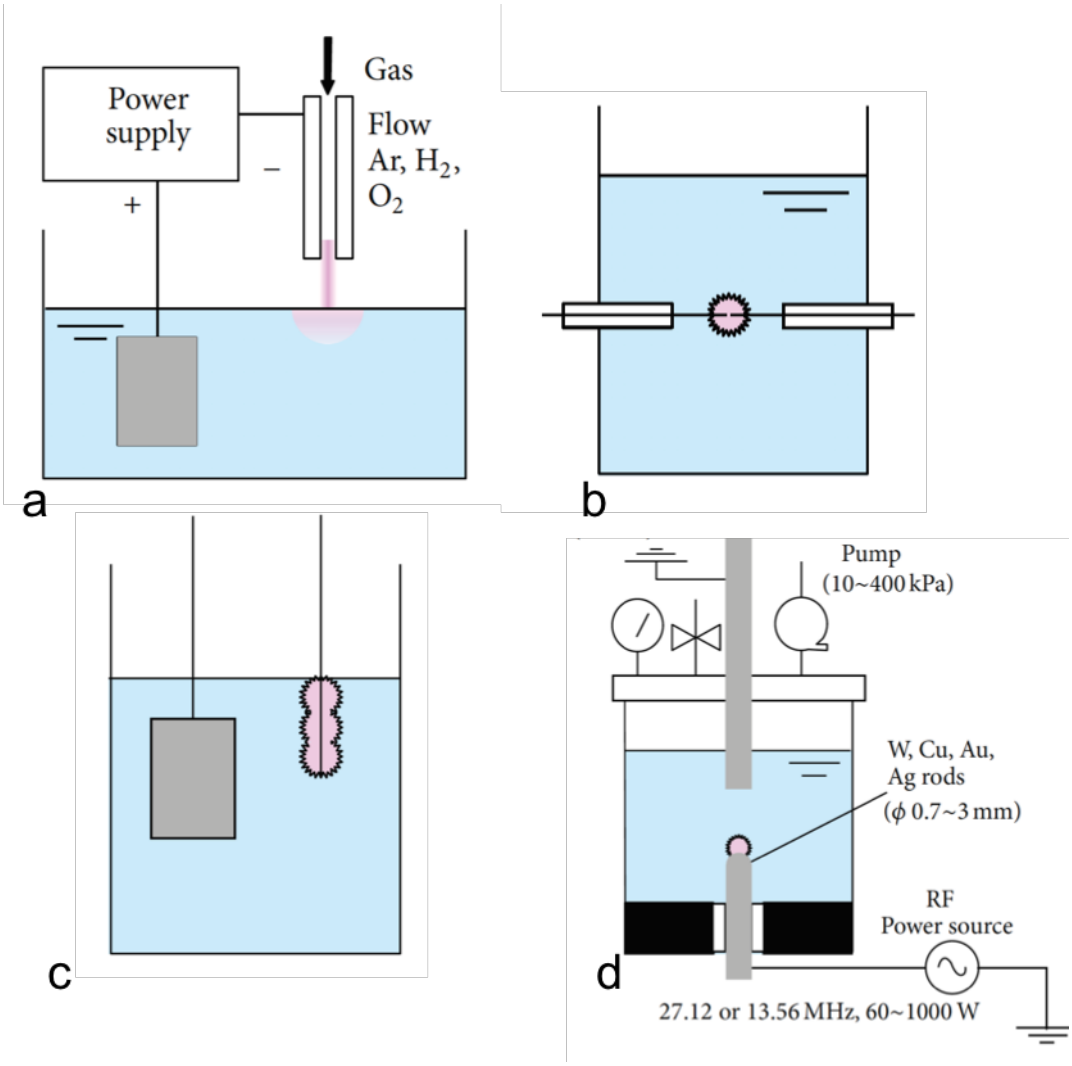

Figure 1.8 Typical setup of plasma generation device for: a) gas discharge between an electrode and electrolyte surface, b) direct discharge between 2 electrodes, c) contact discharge between an electrode and the surface of surrounding electrolyte, d) RF generation.[50]

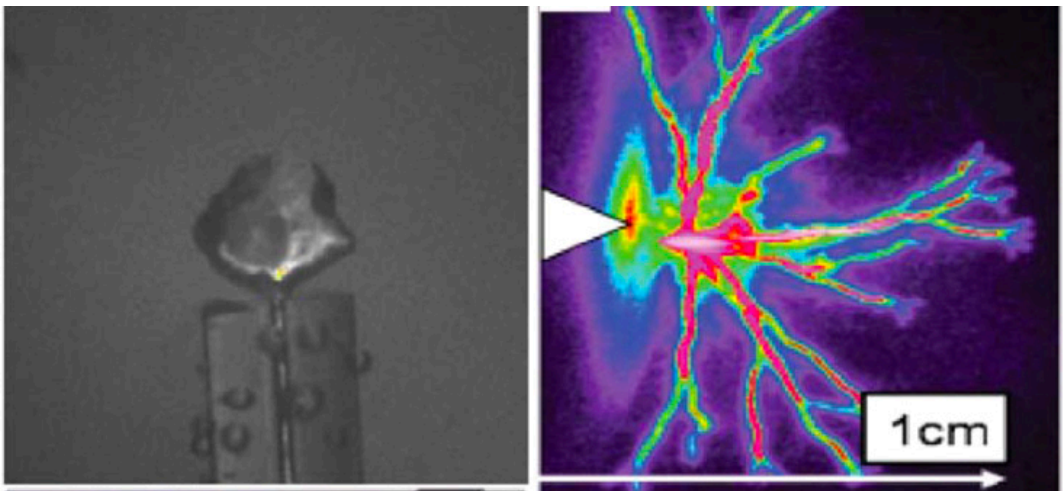

Figure 1.9 Photographs of plasma generated in the bubble and streamer plasma.[52]

1.4.2.1 Difference between RF and MW plasma system

The power is introduced either by radio frequency or microwaves. The system appears almost identical, but their physics is to some extend different. RF system works with frequencies up to the megahertz range, MW systems are in the gigahertz range. Therefore, there is six orders of magnitude less energy transferred to the charged particle in microwave induced plasma as compared to that of RF system. In the RF systems, because of the short free path length of the electrons, the energy of the electrons is in the range of a few eV, whereas the energy of the electrons in microwave plasma is in the range of keV. Electrons with energies of only few eV can attach to the surface of particles. Therefore, in RF systems, NPs are expected to be negatively charged, but in MW systems the electric charge of the particles is positive. The electric charge of the particle is increasing with increasing diameter of the particle.[42]

1.4.2.2 Microwave-induced plasma in liquid process (MWPLP)

Microwave equipment using standard 2.45 GHz frequency become a popular and easy source to produce plasma, due to the high frequency of the microwave irradiation. Microwave generated plasmas have an important advantage over RF plasmas. They have higher frequency oscillations of the electric field, i.e. electrons travel shorter distances compared to RF plasmas before they switch direction. Therefore, fewer electrons reach the device surface per switching cycle, thus minimizing the surface charging effect.[53]

MWPLP is a simple, scalable, and green technique to synthesize nanoparticles which does not need any reducing agents. In this process, plasma discharge occurs with the outbreak of the bubbles (bubble plasma) under normal or reduced pressure.

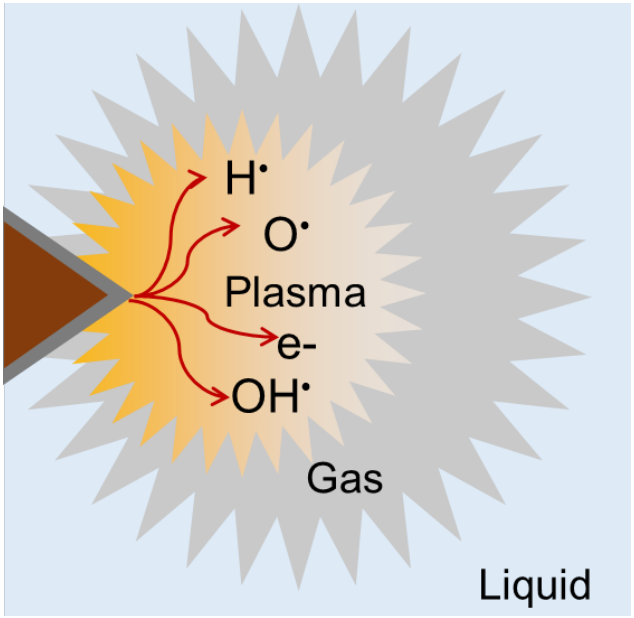

Figure 1.10 Schematic illustration of plasma gas/liquid interface generated in MWPLP.

Plasma is created in 3 steps, in the first step the tip of the electrode is heated by joule heating, which heat surrounding liquid and lead to the outburst of bubbles. In the second stage plasma is initiated at gas (provided by bubbles)/liquid interface, and then in the third stage plasma is formed. Plasma is surrounded by a gas phase in a liquid phase (Figure 1.10), create plasma/gas and gas/liquid interfaces with unique features for the reaction and formation of NPs. After generation of nonequilibrium plasma in water, many reducing and oxidizing species are generated by dissociation, solvation, dimerization and recombination resulting from the decomposition of water molecules (Eq 1, Figure 1.11). Hydrogen radicals, oxygen radicals, and hydroxyl radicals are generated as radicals. Furthermore, strong light and heat as well as electrons are ejected into the system. In these cases, hydrogen radicals and electrons are direct reduction species of metal ions. The solvated electrons ($E°(H_2O/e_{aq}^-)$ = -2.87 V) and hydrogen radicals ($E°(H^+/H•)$ = -2.31 V) are strong reducing species. However, the lifetime of hydrogen radicals should be in the order of ms. Solvated electrons have a longer lifetime in µs. Figure 1.12 shows typical emission spectra during MWPLP, showing presence of hydrogen radicals.

$$H_2O \rightarrow OH• + H• \quad (1)$$

In the second step, the radicals and solvated electrons can react together by dimerization and recombination. In Table 1.1, the possible reactions of the second step are listed. One can easily find that hydrogen molecules (H_2) can be produced

via combination of hydrogen radicals. Secondary formed species such as hydrogen gas molecules can also reduce metal ions after plasma.[51]

Table 1.1 Second step reactions (dimerization and recombination).[51]

Reaction	Reaction rate constant $k/10^{10}$ mol dm^{-3} s^{-1}
$e^-_{aq} + e^-_{aq} \rightarrow H_2 + 2OH^-$	0.54
$e^-_{aq} + H\bullet \rightarrow H_2 + OH^-$	2.5
$H\bullet + H\bullet \rightarrow H_2$	1.3
$e^-_{aq} + H_3O^+ \rightarrow H_2O + H\bullet$	2.3
$e^-_{aq} + OH\bullet \rightarrow OH^-$	3.0
$OH\bullet + OH\bullet \rightarrow H_2O_2$	0.53
$OH\bullet + H\bullet \rightarrow H_2O$	3.2
$H_2O^+ + OH^- \rightarrow 2H_2O$	14.3

e^-_{aq}: Solvated electron ($e- + nH_2O \rightarrow e^-_{aq}$).

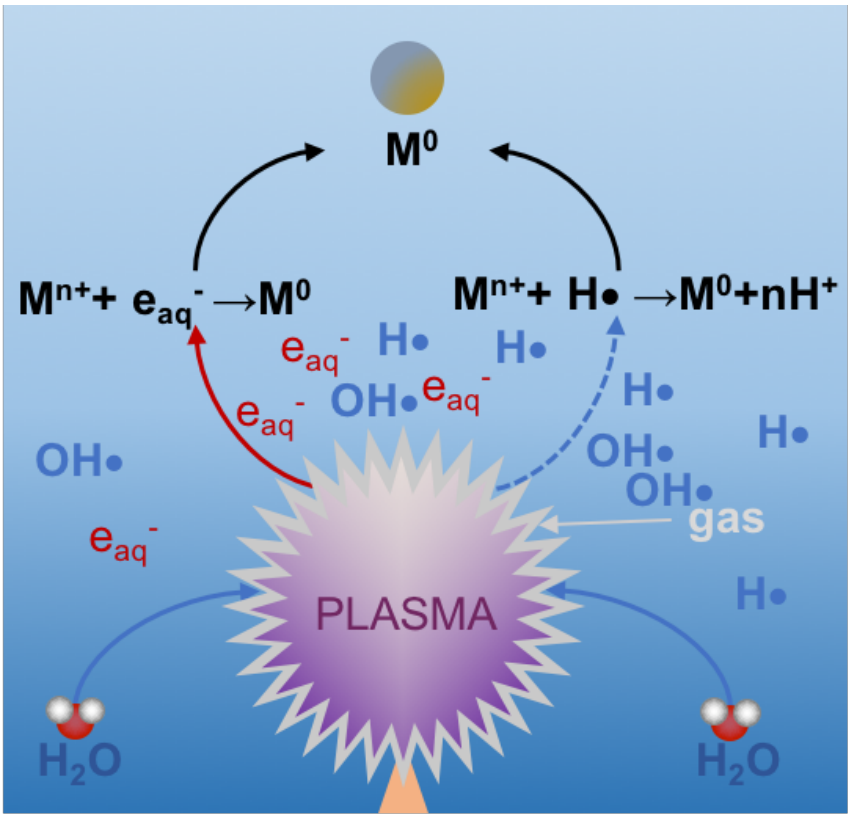

Figure 1.11 Schematic illustration of plasma generated in MWPLP and processes to reduce metal ions.

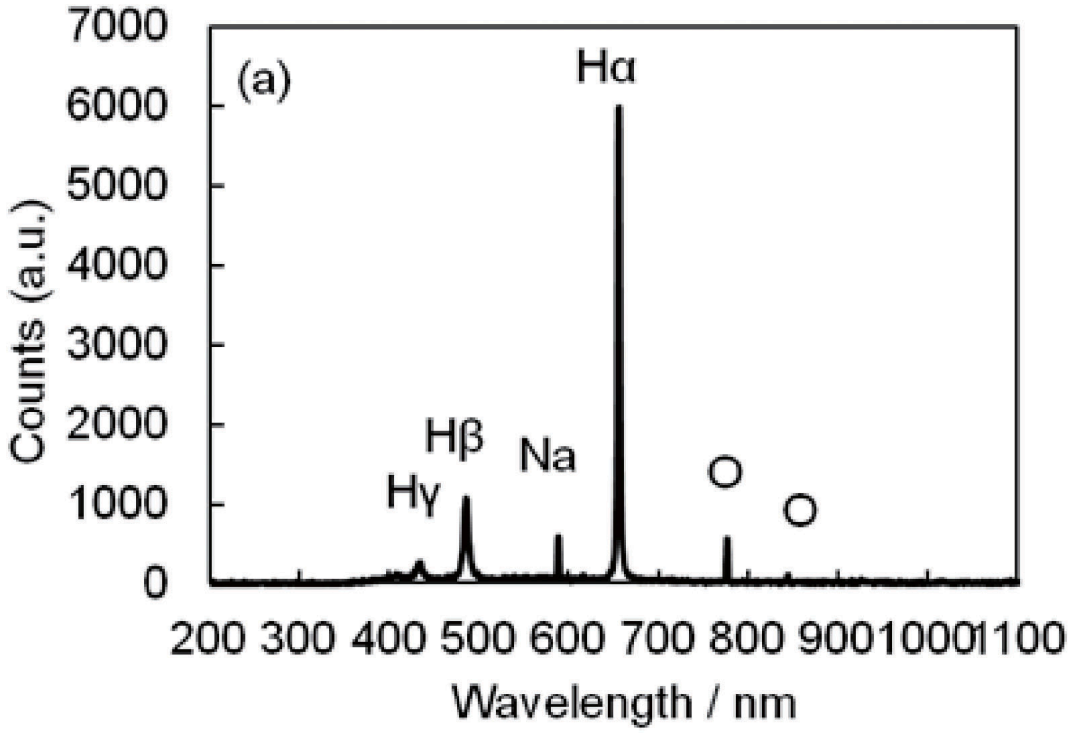

Figure 1.12 Plasma emission spectra[51]

1.4.2.3 Coated electrode in MWPLP

Electrodes which have been conventionally used in plasma in liquid processes are often made of tungsten because of its high melting/boiling point. Electrodes can be made of metals matching the synthesized nanoparticles. Ejection of metal ions or atoms from the electrode by plasma ignition can be observed, even tungsten was used. Ishida et al. reported doping of TiO_2 particles by metal ejected from the tungsten electrode.[35] Therefore, ejection of electrode meterials can contaminate finally produced NPs via plasma reduction of metal salts or metal

complexes, and influence their properties.[30,35] Another example of contamination of the NPs can be found in the fabrication of semiconductor devices. There, in the wafer processing, introduction of high density plasma and plasma cleaning caused formation of contaminated particles.[54]

Use of electrodes as a material source can be one of the effective tools to eliminate such a phenomenon[55], but it has its limits, especially for the noble metal particles in industrial production. Cost efficiency of this method for noble metal particles production in a big scale is not very reasonable.

Second method which can be used to eliminate such a problem is ceramic coating of the electrode surface. This can be a very effective and cost efficient method especially for industrial production of NPs. Ceramic materials are the most promising for the electrode coating due to their great thermo-mechanical and chemical stability. There are several criteria for choosing the right ceramic coating and achieving the best results such as cost, porosity, elution and erosion rate, purity, influence on the electric field, and most importantly plasma resistance. The most common method to estimate plasma resistance of ceramics is to measure etch depth under arbitrary fluorine plasma conditions.[56]

The plasma-resistant ceramics such as alumina (Al_2O_3) and yttrium oxide (Y_2O_3) seem to be a reasonable choice for the selection of affordable and effective

ceramic coating for the electrodes used in plasma since they have been previously used as a processing chamber materials in semiconductors manufacturing.[57] We have selected yttrium oxide as the coating material because of its chemical stability up to 2300 °C and its high thermal stability compared to the alumina or other ceramic materials.[58] Therefore, if the common stainless steel electrode is coated by Y_2O_3, it can lower the damages of the electrode from plasma and extend the lifetime of the electrode with cost efficiency.

In order to eliminate problem related to the contamination of the synthesized NPs, we introduced the ceramic (Y_2O_3)-coated electrode tip in MWPLP (Figure 1.13). In addition, the ceramic layer can enhance the electric field strength on the electrode tip surface, compared with the uncoated electrode, by concentration of the pre-discharge current in small open pores. Thus, many of discharge channels, distributed almost homogenously along the whole surface of the composite electrode, are generated from the pores.[59,60] The plasma generation and NP formation are expected to occur differently from those in the case of using the common un-coated metal electrode.[36] Use of yttrium coated electrode for synthesis of metal and metal alloy NPs was investigated in the chapters 2-5 of this thesis.

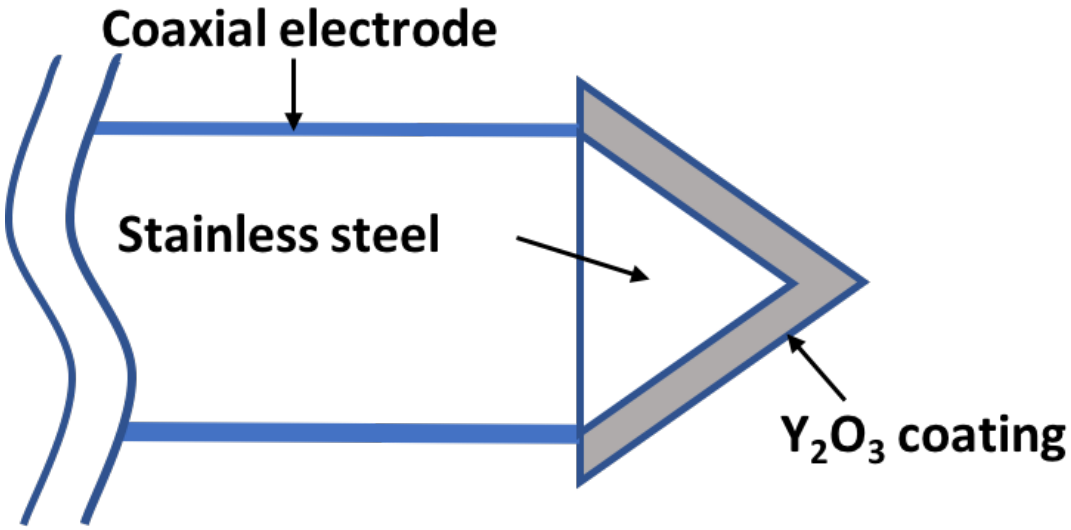

Figure 1.13 Schematic picture of the yttrium oxide (Y_2O_3) electrode tip.[36]

1.5 References

1 T. Yonezawa, T. Tominaga, D. Richard, *J. Chem. Soc., Dalton Trans.*, **1996**, 783.

2 K. Ankireddy, S. Vunnam, J. Kellar, *W. J. Mater. Chem. C*, **2013**, 1, 572.

3 D. V. Talapin, J. S. Lee, M. V. Kovalenko, E. V. Shevchenko, *Chem. Rev.*, **2010**, 110, 389.

4 Y. W. C. Cao, R.C. Jin, C. A. Mirkin, *Science*, **2002**, 297, 1536.

5 W. Fritzsche, T.A. Taton, *Nanotechnology*, **2003**, 14, 63.

6 W. Wenseleers, F. Stellacci, T. Meyer-Friedrichsen, T. Mangel, C.A. Bauer, S.J.K. Pond, S.R. Marder, J. W. Perry, *J. Phys. Chem. B*, **2002**, 106, 6853.

7 X. Yin, N. Fang, X. Zhang, I. B. Martini, B. J. Schwartz, *Appl. Phys. Lett.*, **2002**, 81, 3663.

8 A. Akbarzadeh, M. Samiemi, S. Davaran, *Nanoscale Res Lett.*, **2012**, 7, 144.

9 V. V. Mody, R. Siwale, A. Singh, H. R. Mody, *J Pharm Bioallied Sci.*, **2010**, 2, 282.

10 F. Zhu, J. Kim, K.-C. Tsao, J. Zhang, H. Yang, *Curr. Opin. Chem. Eng.*, **2015**, 8, 89.

11 Y. S. Kang, S. Risbud, J. F. Rabolt, P. Stroeve, *Chem. Mater.*, **1996**, 8, 2209.

12 Q. A. Pankhurst, J. Connolly, S. K. Jones, J. Dobson, *J. Phys. D.: Appl. Phys.*, **2003**, 36, R167.

13 J. Dobson, *Gene Ther.*, **2006**, 13, 283.

14 S. Rudge, C. Peterson, C. Vessely, J. Koda, S. Stevens, L. *Catterall, J. Control. Release*, **2001**, 74, 335.

15 N. Harris, M. J. Ford, P. Mulvaney, M. B. Cortie, *Gold Bull.*, **2008**, 41, 5.

16 M. B. Cortie, X. Xu, M. J. Ford, *Phys. Chem. Chem. Phys.*, **2006**, 8, 3520.

17 J. Wilcoxon, *J. Phys. Chem. B*, **2009**, 113, 2647.

18 T. Udayabhaskararoo, Y. Sun, N. Goswami, S. K. Pal, K. Balasubramanian, T. Pradeep, *Angew. Chem., Int. Ed.*, **2012**, 51, 2155.

19 A.-Q. Wang, J.-H. Liu, S. D. Lin, T.-S. Lin, C.-Y. Mou, *J. Catal.*, **2005**, 233, 186.

20 B. Xia, F. He, L. Li, *Langmuir*, **2013**, 29, 4901.

21 X. Ren, X. Meng, F. F. Tang, *Sens. Actuators B*, **2005**, 110, 358.

22 N. Toshima, T. Yonezawa, *New J. Chem.*, **1998**, 22, 1179.

23 E. Moncada, R. Quijada, J. Retuert, *Nanotechnology*, **2007,** 18, 335606.

24 R.S. Dubey, Y.B.R.D. Rajesh, M.A. More, *Mater. Today - Proc.*, **2015**, 2, 3575.

25 M. Brust, J. Fink, D. Bethell, D. J. Schiffrin, C. Kiely, *J. Chem. Soc., Chem. Commun.*, **1995**, 0, 1655.

26 B. S. Zelakiewicz, T. Yonezawa, Y. Tong, *J. Am. Chem. Soc.*, **2004**, 126, 8112.

27 D. Lopez, I.Y. Abe, I. Pereyra, *Diam. Relat. Mater.*, **2015**, 52, 59.

28 X. Guo, K. Gao, A. Gutsche, M. Seipenbusch, H. Nirschl, *Powder Technol.*, **2015**, 272, 23.

29 A. Galvez, N. Herlin-Boime, C. Reynaud, C. Clinard, J.-N. Rouzaud, *Carbon*, **2002,** 40, 2775.

30 S. Sato, K. Mori, O. Ariyada, H. Atsushi T. Yonezawa, *Surf. Coat. Tech.*, **2011**, 206, 955.

31 M.A. Bratescu, S.-P. Cho, T. Osamu, N. Saito, *J. Phys. Chem. C*, **2011**, 115, 24569.

32 Y. Hattori, S. Mukasa, H. Toyota, T. Inoue, S. Nomura, *Mater. Lett.*, **2011**, 65, 188.

33 H. Lee, S. H. Park, J. J. Kim, Y. K. Park, B. H. Kim, S. C. Jung, *Microelectron. Eng.*, **2015**, 126, 153.

34 Y. Hattori, S. Nomura, S. Mukasa, H. Toyota, T. Inoue, T. Kasahara, *J. Alloy. Compd.*, **2013**, 560**,** 105.

35 Y. Ishida, Y. Motokane, T. Tokunaga and T. Yonezawa, *Phys. Chem. Chem. Phys.,* **2015,** 17, 24556.

36 D. Čempel, M. T. Nguyen, Y. Ishida, Y. Wang, K.C.-W. Wu, T. Yonezawa, *J. Nanosci. Nanotechnol.*, **2016**, 16, 9257.

37 M. Nishimoto, H. Tsukamoto, M. T. Nguyen, T. Yonezawa, *ChemistrySelect*, **2017**, 2, 7873.

38 L. Tonks, I. Langmuir, *Phys. Rev*, **1929**, 33, 195.

39 D.V. Szabo, S. Schlabach, *Inorganics*, **2014**, 2, 468.

40 Gotaquestion, **2013**, availiable from: *https://physics.stackexchange.com/q/79462*.

41 O. Takai, *Pure Appl. Chem.*, **2008**, 80, 2003.

42 D. Vollath, *Kona,* **2007**, 25, 39.

43 O.L. Li, N. Takeuchi, Z. He, Y. Guo, K. Yasuoka, J.S. Chang, N.Saito, *Plasma Chem. Plasma Process.*, **2012**, 32, 343.

44 N. K. V. Vel Leitner, G. Syoen, H. Romat, K. Urashima, J.S. Chang, *Water Research*, **2005**, 39, 4705.

45 M. Sato, T. Ohgiyama, J. S. Clements, *IEEE Trans. Ind. Appl.*, **1996**, 32, 106.

46 J. Hieda, N. Saito, O. Takai, *J. Vac. Sci. Technol. A.*, **2008**, 26, 854.

47 G. Saito, S. Hosokai, M. Tsubota, T. Akiyama, *J. Appl. Phys.*, **2011**, 110, 330.

48 S.P. Cho, M. A. Bratescu, N. Saito, O. Takai., *Nanotechnology*, **2011**, 22, 455701.

49 K. Kim, *J. Cryst. Grow.*, **2005**, 283, 540.

50 G. Saito, T. Akiyama, J Nanomater., **2015,** Article ID 123696.

51 H. Shirai, M. T. Nguyen, D. Čempel, H. Tsukamoto, T. Tokunaga, Y.-C. Liao, T. Yonezawa, *Bull. Chem. Soc. Jpn.*, **2017,** *90*, 279.

52 Q. Chen, J. Li, Y. Li, *J. Phys. D: Appl. Phys.*, **2015**, 48, 424005.

53 Pvatepla America, **2016**, availiable from: *http://www.pvateplaamerica.com/admin/contents/semi_whymicrowave_text_1.html*

54 G. S. May, C. J. Spanos, *IEEE*, **2006,** 98.

55 Y. Ishida, S. Motono, W. Doshin, T. Tokunaga, H. Tsukamoto, T. Yonezawa, *ASC Omega*, **2017**, 2, 5104.

56 D. M. Kim, K. B. Kim, S. Y. Yoon, Y. S. Oh, H. T. Kim, S. M. Lee, *J. Ceram. Soc. Jpn.*, **2009**, 117, 863.

57 J. Iwasawa, R. Nishimizu, M. Tokita, M. Kiyohara, K. Uematsu, *J. Am. Ceram. Soc.*, **2007**, 90, 2327.

58 D. H. Kuo, W. R. Chen, *Thin Solid Films*, **2006**, 497, 65.

59 P. Lukes, M. Clupek, V. Babicky, P. Sunka, *IEEE Trans. Plasma Sci.*, **2008**, 36, 1146.

60 P. Lukes, M. Clupek, P. Sunka, V. Babicky, *Czech. J. Phys.*, **2002**, 52, 800.

1.6 Purpose of this study

Microwave-induced plasma in liquid process has many advantages to produce nanoparticles. Especially, relatively rapid reduction caused by the radicals formed during plasma process by decomposition of water. Liquid-plasma has been investigated intensively by several groups for over a decade now, however, many problems are still remaining, and mechanisms of particle formation are quite unknown.

Problems

(1) Contamination of the finally produced nanoparticles by electrode materials.

(2) The parameters that are essential for controlling the size and composition of various nanomaterials have not been well understood.

(3) Unknown mechanism of particle formation.

Purpose of this study

The purpose of this study is to solve the above-mentioned problems of solution plasma synthesis of nanomaterials. Use coated electrode as a plasma source in the MWPLP, protect finally produced nanoparticles from contamination from the

electrode materials, this significantly improve use of metal salts as precursors in liquid-plasma. This thesis includes five chapters:

Chapter 1 presented a general introduction. The objective and strategy of the research in this thesis using coated electrode in MWPLP.

Chapter 2 described the Au nanoparticles formation in MWPLP using coated electrode and influence of solution pH on the particles size and size distribution.

Chapter 3 described the study on synthesis of Ag nanoparticles influenced by initial silver precursor choice and by various amount of used L-arginine.

Chapter 4 described the strategy for ligand free synthesis of bimetallic alloy Au/Ag nanoparticles in MWPLP.

Chapter 5 presented the general conclusions of this thesis.

2 Au nanoparticles prepared using a coated electrode in plasma-in-liquid process: Effect of the solution pH

2.1 Introduction

Currently, metal nanoparticles (NPs) are under immense interest because of their unique optical, electrical, and catalytic properties.[1-5] They are used in variety of applications such as electronics,[6] photodynamic therapy,[7] therapeutic agent delivery,[8] sensors,[9] probes,[10] diagnostics,[11] catalysis,[12,13] and material for laser

desorption/ionization mass spectroscopy.[14] Among various metal NPs, gold NPs are most studied and they have been used in numerous applications from jewelry to advanced technology and medicine.[4,15,16] Several methods have been established to synthesize gold NPs, including chemical reduction,[17,18] laser ablation,[19] and vacuum sputtering.[2,5,20] Chemical reduction, the most common way to produce gold NPs require the use of reducing agents (alcohol, $NaBH_4$, N_2H_4, citrate, polyol, etc.) or stabilizing agents, which are sometimes toxic and not environmentally friendly.

In contrast, microwave induced plasma in liquid process (MWPLP) is a simple, scalable, and green technique to synthesize NPs which does not need any reducing agents.[21] In this process, plasma discharge occurs with the outbreak of the bubbles under normal or reduced pressure. Plasma is surrounded by a gas phase in a liquid phase, create plasma/gas and gas/liquid interfaces with unique features for the reaction and formation of NPs.[22,23] The produced nonequilibrium plasma provides various reactive chemical species (e.g., hydrogen radicals, hydroxyl radicals, and oxygen radicals from water) and UV radiation, that can reduce metallic ions in extremely rapid reactions in confined areas.

Using PLP, NPs of various metals and metal oxides such as Au,[23] Ag,[22] Pt,[22] Zn,[24] Sn,[25] ZnO,[24] SnO_2,[25] and WO_3[26] have been prepared. In most cases, plasma in liquid processes are using tungsten electrode because of its high melting / boiling points or the electrode of metals corresponding to the NPs. Ejection of metal ions or atoms from the electrodes can be observed by plasma ignition, even tungsten was used. In some reports, electrodes play a role of the raw materials for NPs formation. However, such metal electrodes can contaminate finally produced NPs,

influence their intrinsic properties.[22,27] In order to eliminate this problem, our present research focuses on the use of ceramic (Y_2O_3)-coated electrode to synthesize metal NPs: the preparation of gold NPs was taken into account as a case study. Using the ceramic-coated electrode, the ceramic layer help redistribute the electric field on the electrode during pre-discharge phase. The electric-field strength on the surface of the coated electrode is many times enhanced in comparison with metallic uncoated electrode.[28] This electric-field enhancement initiates a large number of discharge channel which are almost homogenously distributed along the whole surface of the coated electrode tip. The plasma generation and NP formation are expected to occur differently from those in the case of using the common un-coated metal electrode. Therefore, using the ceramic-coated electrode, we investigate the time-dependent formation and growth of gold NPs during PLP. In addition, we also elucidate the effect of the solution pH on gold NPs in terms of their size and size distribution, which exhibit a very different manner in comparison to that in the case of using uncoated electrode.

2.2 Aim of this chapter

This chapter is focusing on preparation of gold nanoparticles microwave-induced plasma-in-liquid process (MWPLP). In order to overcome one of the current challenges associated with the impurity produced from metal electrodes, study in this chapter utilized a ceramic-coated electrode to prepare pure Au NPs stabilized by L-arginine. Using this electrode, the reduction of Au ions during the plasma irradiation, the formation of Au NPs, their size and size distribution as a

function of the pH were investigated. Our results show that a bimodal NP size distribution was obtained at pH 3.5 – 12.0. The fraction of small sized Au NPs becomes significant at pH 6.0 and 12.0 while that of big sized Au NPs is dominant at pH 3.5. The results in this chapter suggested that this change in the size distribution of Au NPs was governed by the reduction rate of gold ion at different pH under plasma generated in water.

2.3 Experimental section

2.3.1 Apparatus

The schematic illustration of solution plasma reactor is shown in Figure 2.1a.[22,27,29] Microwaves (2.45 GHz) are emitted from magnetron (Micro denshi UW-1500) and pass through a WRJ-2 rectangular waveguide (109.22 × 54.61 mm), a power meter, a tuner, a waveguide to the coaxial adaptor, and plasma source. The coaxial electrode is attached in the middle of waveguide and her front is projected in to the chamber. This coaxial electrode is ended by an Y_2O_3-coated stainless steel sharp tip (Figure 2.1b). The stainless steel reactor (500 cm^3) is coated inside with PTFE. Plasma solution is cooled by a stainless cooling spiral with chilled liquid at 5 °C. Plasma ignition and the solution during plasma reaction can be observed by eye through the quartz window. Pressure was decreased by a diaphragm vacuum pump and measured by a vacuum gauge.

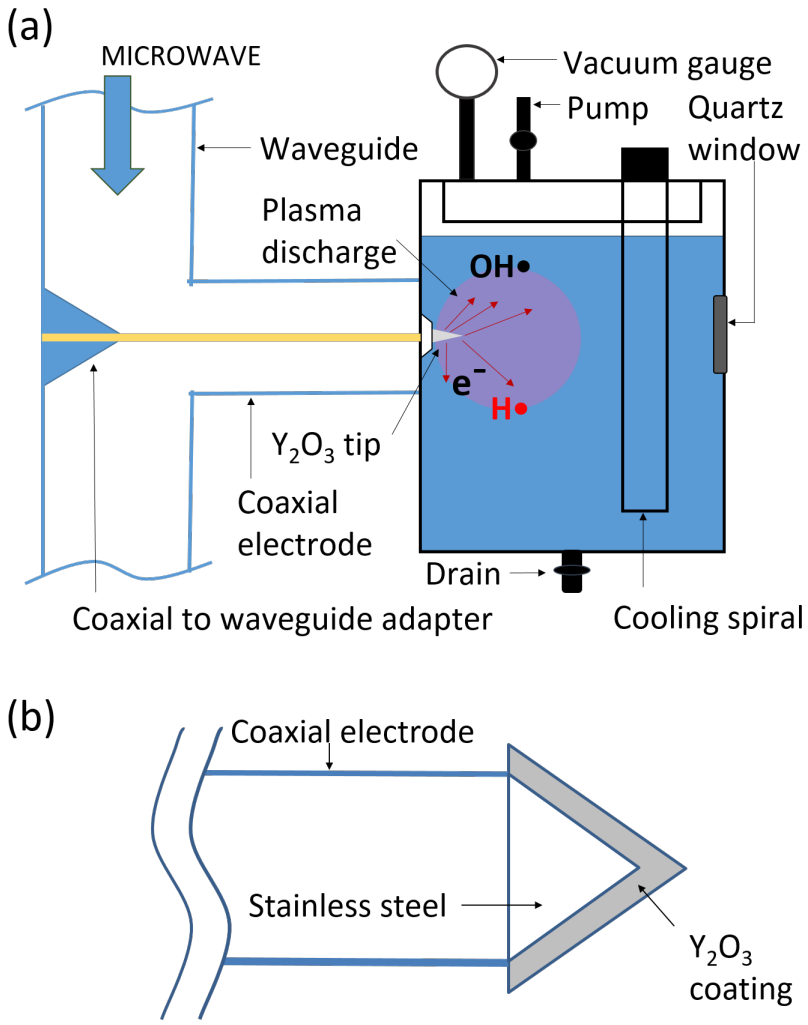

Figure 2.1 (a) Schematic illustration of the plasma reactor of microwave induced plasma-in-liquid process used in this study and (b) configuration of the Y_2O_3-coated stainless steel electrode.

2.3.2 Materials

Tetrachloroauric(III) acid hydrate ($HAuCl_4 \cdot nH_2O$ n=3.6, Kojima Chemicals, Japan) and L-arginine ($C_6H_{14}N_4O_2$, Junsei Chemical, Japan) were used as a precursor and a stabilizer, respectively. Potassium bromide (KBr, Ohyo Koken

Kogyo, Japan) was used to make complex ($AuBr_4^-$) in order to detect the unreacted Au^{3+} ions. Sodium hydroxide (NaOH, 97%, GR grade, Junsei), and hydrochloric acid (HCl, 35-37%, Junsei) was used for pH adjustment. All chemicals were used as received. The deionized water (Organo/ELGA purelabo system, > 18.2 MΩ·cm) was used to prepare solution for plasma reaction.

2.3.3 Synthesis of Au NPs

5.02 cm^3 of aqueous $HAuCl_4$ (0.050 M) was added into 500 cm^3 of water, followed by the addition of 1.74 cm^3 of aqueous L-arginine (0.287 M). The molar ratio of Au and L-arginine was 1:2. The mixed solution was stirred for 10 minutes, and then introduced into the reaction vessel. The plasma was initiated at 650 W of the microwave output. Then, in order to keep plasma generation, the output was kept at 400 W during whole reaction. The plasma reaction was allowed for occurring for 140 min.

2.3.4 Characterizations

UV-Vis spectra were collected in order to observe reduction of Au^{3+} ions and formation of Au NPs using an UV-Vis spectrophotometer (Shimadzu UV-1800) and a quartz cell with 1 cm optical path. During plasma reaction, 3 cm^3 of the sample solutions were taken directly from the plasma chamber for each measurement at various reaction time, and 0.012 mmol of KBr was added into the sample solution

and pH the taken samples was adjusted to around pH 3 by addition of 1 M HCl solution.

The transmission electron microscopy (TEM, JEOL JEM 2000-ES, at 200 kV) with an energy dispersive X-ray spectroscope (EDS) was used to analyze the morphology and elemental composition of the obtained Au NPs. For preparation of TEM samples, NP dispersions were filtered using a membrane filter (pore size = 0.2 μm), then re-dispersed in water with a sonicator. After that these purified Au NP dispersions were dropped on collodion film-coated copper TEM grids, and naturally dried. More than 100 NPs was used to estimate the particle size in arbitrary chosen areas and size distribution using TEM images. A part of the filtrated NPs was examined with X-ray diffraction (XRD, Rigaku MiniFlex II, Cu Kα radiation, scanning rate of 5 ° min^{-1}).

2.4 Results and discussion

2.4.1 Study of time dependent reduction of gold(III) ions and formation of Au NPs at different pH: UV-Vis spectra

L-arginine is an amino acid which is used as a stabilizing agent for the preparation of Au NPs. It has an isoelectric constant of 10.87. Depend on the pH of the solution, L-arginine exhibits negative (pH 12.0) or positive charge (pH 3.5 and 6.0). In either the case, it can stabilize NPs from severely aggregation in the studied pH range (3.5-12.0) via its adsorption on Au NP surface and creation of a layer for the repulsive interaction between NPs.

Since the position and intensity of the surface plasmon resonance (SPR) peak for Au NPs can vary according to the size and aggregation of Au NPs. However, using SPR peak may not be quantitative to determine the degree of reduction of Au ions. In this study, reduction rates of Au^{3+} ions during plasma-in-liquid process were evaluated. In order to detect the reduction of Au^{3+} ion, KBr was added into the taken-out sample liquids from the reaction solutions during plasma reduction in order to form a complex, $AuBr_4^-$, instead of the raw material complex $AuCl_4^-$. The absorption coefficient of the peak at ca. 380 nm of $AuBr_4^-$ is much higher than that of $AuCl_4^-$.

UV-Vis spectra in Figures 2.2a-c showed that an increase in plasma reaction time resulted in the decrease of UV-Vis absorption peak area (380 nm) of $AuBr_4^-$ complex, which reflected more Au^{3+} ions being reduced. The complete reduction of Au^{3+} to Au(0) was obtained after 140 min when the absorption peak of $AuBr_4^-$ disappeared. The ratio (A/A_0) between the absorbance peak area (A) at reaction time $t = 0 – 140$ min and that (A_0) at $t = 0$ (Figure 2.2d) indicated the reduction rate of Au complexes when using solution with pH 3.5-12.0 during 140 min plasma discharge. The reduction rate decreased with an increase in pH from 3.5 to 12.0. It was observed for all studied pH that the reduction of Au complexes proceeded significant for the first 20 min discharge, then decreased with prolonging the reaction time. In Figure 2.2d, it is clear that it took about 20, 60, and 100 min respectively for the reduction of about 80 % Au complexes for pH 3.5 to 6.0 and to 12.0, respectively. After 140 min plasma discharge, more than 89 % of Au complexes were reduced for pH 12.0, and more than 99 % of Au complexes were reduced for pH 3.5 and 6.0.

It is known that depend on the initial pH of the solution, different degree of hydrolysis of $AuCl_4^-$ can occur (Eq. 1) with $x = 0 - 4$:[30]

$AuCl_4^- + xOH^- \rightarrow AuCl_{4-x}(OH)_x^- + xCl^-$ (Eq. 1)

The reduction of gold ion by the plasma produced hydrogen radical followed different ways at different pH values:[23]

At low pH (e.g. pH 3.5):

$AuCl_4^- + 3H\cdot \rightarrow 3HCl + Au^0 + Cl^-$ (Eq.2)

And at high pH (e.g. pH 12.0):

$Au(OH)_4^- + 3H\cdot \rightarrow 3H_2O + Au^0 + OH^-$ (Eq. 3)

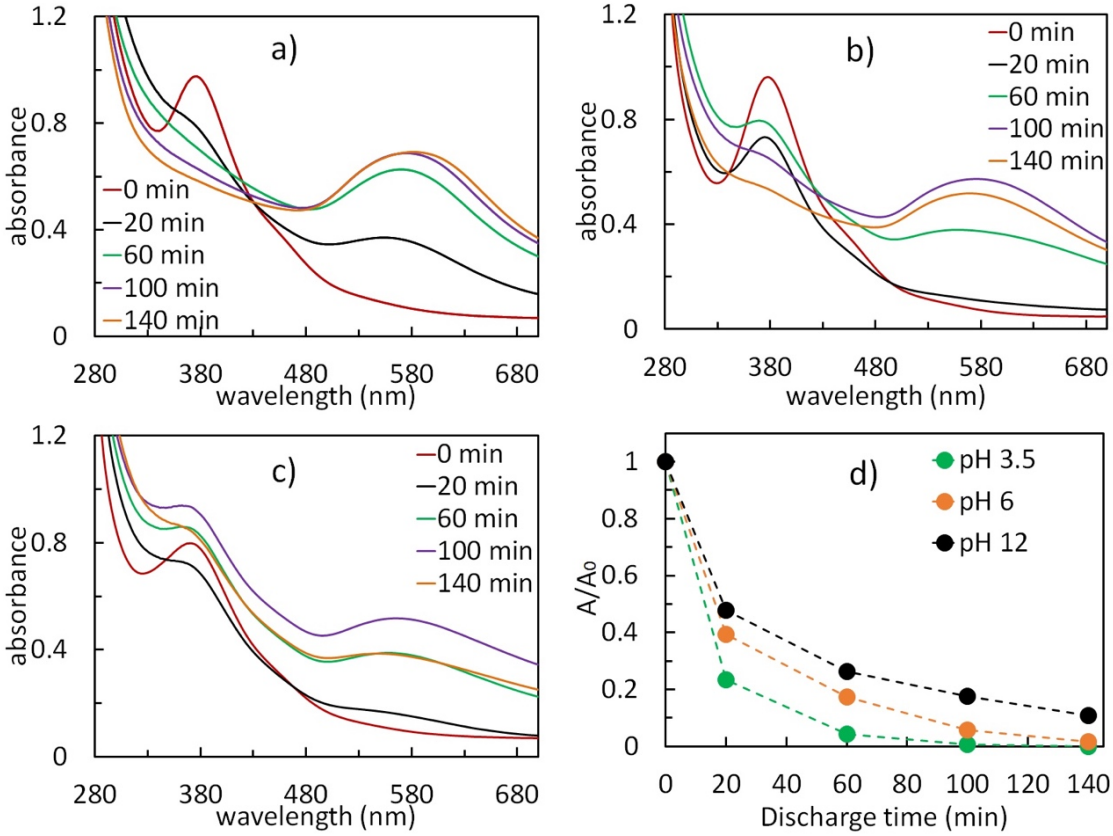

Figure 2.2 (a-c) Time dependent UV-Vis spectra during plasma reaction to form Au NPs in aqueous solution with pH a) 3.5, b) 6.0, and c) 12.0. (d) Plot of A/A0 as function of reaction time for pH 3.5 - 12.0. A: The peak area of the absorption of $AuBr_4^-$ at ca. 380 nm during plasma discharge. A_0: The peak area of the absorption of $AuBr_4^-$ at ca. 380 nm before plasma irradiation.

The reduction of $AuCl_4^-$ ion to Au(0) shows higher reactivity than the that of $Au(OH)_4^-$ to Au(0) (see Figure 7, Ref. 31). Therefore, the reduction rate of Au^{3+} ions decreases when pH of the reaction solution increases. Previous study also suggested a higher reduction speed for gold ion at lower pH in the initial period of

the reaction course.[31] In addition, the pH of the solution after 140 min plasma discharge (Table 2.1) showed that the pH dropped (12.0 to 11.8) for sample prepared from solution with pH 12.0. This decrease in pH indicates that protons were changed from hydrogen radicals generated by plasma. For reaction solution with initial pH 6.0, after 140 min discharge, pH significantly decreased (6.0 to 3.7). A pH drop was also found in case of solution with pH 3.5 (3.5 to 3.1). Similar results of pH drops were reported with using pulse discharge with uncoated electrode in synthesis of Au NPs.[23]

Figures 2.2a-c also show that the SPR peak centered at 560 nm of Au NPs was observed and increased in the intensity with prolong plasma reaction. The SPR peaks were observed at longer wavelength than the fingerprint SPR peak position for Au NPs at 520 nm, suggesting some aggregations of Au NPs were generated in the reaction solutions during plasma irradiation. Some aggregated structures can be found in some TEM images (see Figure 2.3). When the plasma irradiation was performed with the reaction solution at pH = 3.5 (Figure 2.2a), the formation of Au NPs indicated by the SPR peak at 560 nm can be observed after 20 min plasma irradiation. When we used the reaction solution at pH = 6.0 and 12.0 (Figures 2.2b-c), the SPR peak was not clearly observed after 20 min reaction despite the fact that the Au^{3+} was reduced. In these cases, after 60 min plasma irradiation, the SPR peak of Au NPs clearly appeared in the spectrum. These results indicate that when the plasma irradiation was performed at lower pH of the solution, the formation of plasmonic Au NPs occurred more rapidly than at a higher pH. This corresponds to the reactivity of Au^{3+} at different pH under plasma irradiation.

2.4.2 Transmission electron microscopy observation for pH dependent size and size distribution of Au NP

TEM images of Au NPs after 140 min reaction at pH 3.5, 6.0, and 12.0 and their size distributions are shown in Figures 2.3a–f. In all cases, NPs presented in the TEM images exhibit the bimodal size distributions. These results are consistent with the broadening of SPR absorption observed in UV–Vis spectra (Figures 2.2a-c). The bimodal size distribution are also found after 20 min plasma irradiation (Figures 2.3g–k). The existence of small NPs with size less than 5 nm and bigger NPs of ten to several ten nm can be found in Figures 2.3g–k. It is corresponding to the plasmon peak of Au NPs can be found in UV–Vis spectra after 20 min plasma irradiation. The size of small Au NPs obtained for all pH is similar (2.1 – 3.4 nm). The fraction of large NPs obtained at pH = 12.0 is less and their sizes are smaller than the large NPs obtained at pH = 3.5. And the amount of the large NPs obtained at pH = 6.0 is almost negligible while their sizes are larger than other samples. The difference in contrast observed for the big Au NPs could come from the boundaries of the twin planes (decahedron Au NPs, inset of Figure 3b, Figure 2.3c) or different crystal grains (Figures 2.3a and 2.3g) in a single NP, exhibited polycrystalline structure of big Au NPs.

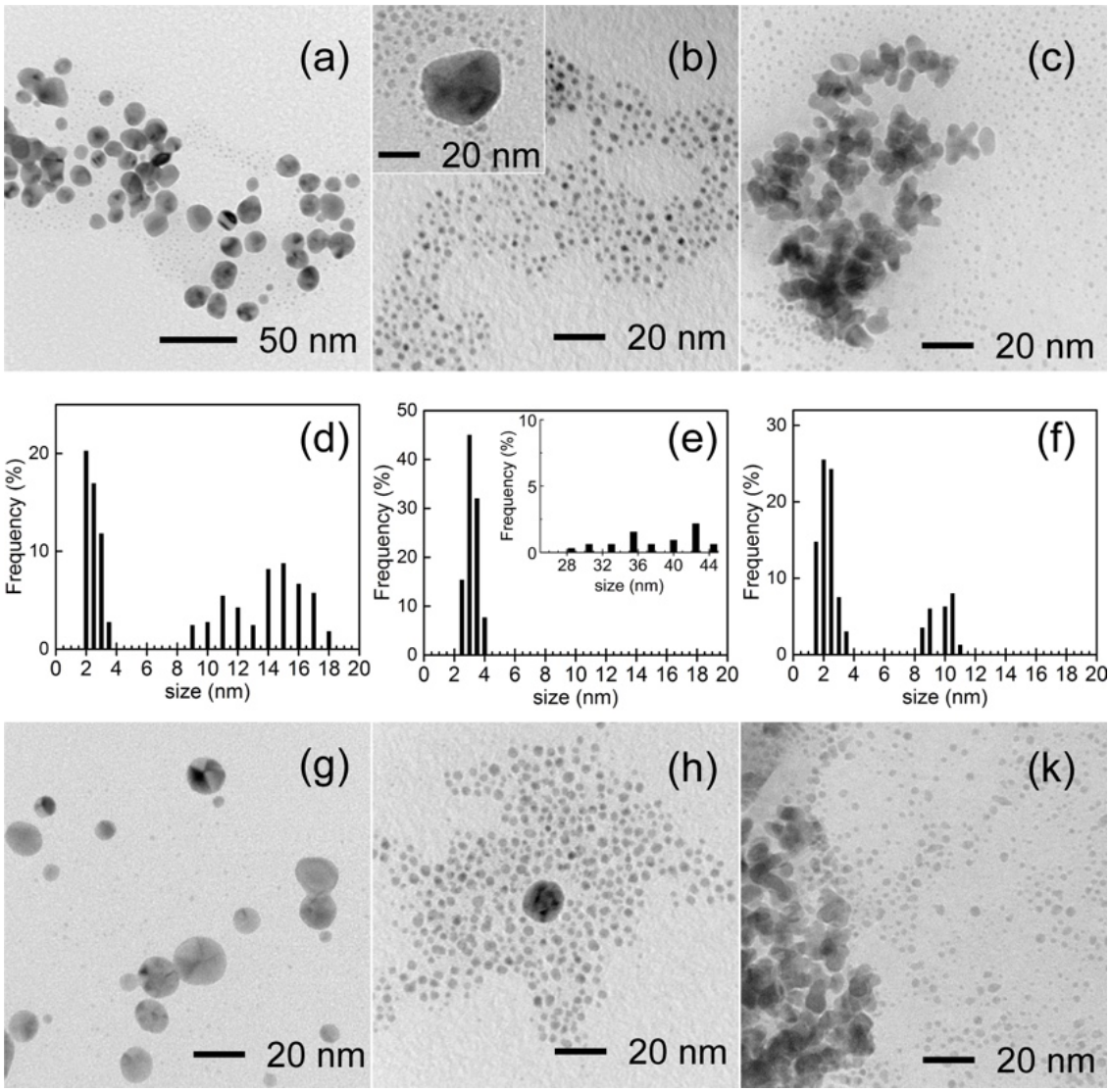

Figure 2.3 TEM images and size distributions of Au NPs obtained after 140 min reaction at different pH: (a, d) pH 3.5, (b, e) pH 6.0, and (c, f) pH 12.0. (g-k) TEM images of Au NPs obtained after 20 min at pH 3.5, 6.0 and 12.0 respectively. In set of (b) shows a big Au NP among smaller Au NPs. Inset of (e) shows the size distribution of big Au NPs.

In citrate reduction method, the formation mechanism of Au NPs was reported depending on pH of the reaction solution.[31] At low pH (acidic) the fast reduction

occurs, followed by nucleation, aggregation, and intra-particle ripening, results in smooth spherical Au NPs. Change to more basic conditions, the reduction of Au complexes becomes slower, two step of NP formation, i.e. nucleation and slow-growth, dominantly controls the particle size and size distribution. In our case, at pH 3.5, the relatively high reduction speed of $AuCl_4^-$ ion complexes to Au(0) can somehow create the supersaturation and aggregation of nuclei and atoms, lead to the formation of large fraction of big NPs. Different from the conventional citrate reduction (reduction completed within a minute)[31] or the PLP using uncoated electrode,[23] the obtained bimodal size distribution at pH 3.5 in our case was thought due to the lower reduction speed that occurs in PLP using coated electrode at room temperature with low concentration of Au complex solution. These conditions can support the uncompleted aggregation step in the formation mechanism and stabilization of small sized Au NPs by L-arginine. As a result, small NPs still exist in the reaction solution during the reaction course. Of course, the non-homogeneity of the reaction solution (no stirring) can also be the reason. An increase in pH led to the increase in the fraction of small sized NPs. Bratescu et al. reported Au NP size dependence on the solution pH using uncoated Pt electrodes in a plasma pulse discharge in liquid. They observed decrease in the NPs size with increase of the solution pH. The lower reduction speed (Figure 2.2d) at high pH reduces the supersaturation and severe aggregation of atoms and nuclei. As a result, small sized NP fraction becomes dominant at high pH, similar to the small NPs observed using uncoated electrode even though the bimodal size distribution wasn't observed.[23] The main difference between NPs formed in PLP by pulse discharge with NPs formed using uncoated electrodes is that a strong dependence between

pH and particle size was not observed in our case, instead we could observe a redistribution of the number of big and small NPs with pH. Other authors also commented that in the basic environment the repulsive interaction was stronger for citrate stabilized Au NPs,[32] this could somehow prevent the aggregation step during NP growth. In our case, carboxyl group in L-arginine can adsorb onto NP surface and provide a similar stabilizing function in basic conditions. However, on the other hand, low reduction rates in the present study could cause the uncomplete separation between nucleation and growth and a heterogeneous growth of NPs could occur in the system. Therefore, the existence of big sized Au NPs as a minor fraction at pH (6.0-12.0) was also observed.

Table 2.1 Mean diameters of Au NPs obtained by plasma irradiation at different pH values of the reaction solution.

pH before plasma irradiation	**pH after plasma irradiation[a]**	**Particle diameter / nm**	
		Small NPs	**Large NPs**
3.5	3.1	2.4±0.4	13.5±2.0
6.0	3.7	3.1±0.4	38.1±4.1
12.0	11.8	2.1±0.4	9.7±0.7

[a]pH values of the reaction solutions after 140 min plasma irradiation

2.4.3 X-ray diffraction patterns, energy dispersed X-ray spectra of Au NPs, and influence of the coated electrode on the NPs purity

Using conventional electrodes in PLP which are often made of tungsten, platinum or other metals with high melting/boiling point can lead to the ejection of the metal ions from the electrode by plasma, and thereby to the contamination of finally produced NPs. [22,23,27,33] Ishida et al. have reported doping of the TiO_2 NPs by ejected metal ions from the tungsten electrode.[27] High demand of the highly pure metallic NPs especially in the semiconductors industry and medicine requires new, cheap solutions for mass production of these NPs.[34]

X-ray diffraction (XRD) pattern and energy dispersed X-ray spectra (EDS) of Au NPs prepared by PLP at pH = 3.5 are collected in Figure 2.4. XRD pattern showed only signals from metallic gold. EDS spectrum also showed characteristic peaks of Au (Cu peaks belong to the grid) without any other elements from the electrode. These results exhibit a high purity of the resulting Au NPs, and it is the advantage of the PLP with the use of ceramic coated electrodes for metal NP preparations. This is consistent with the low elution and erosion rate of the Y_2O_3 coating. The Y_2O_3 coating has the best plasma resistance which is often investigated by measuring the etching depth under arbitrary fluorine plasma conditions.[35] This coating has high chemical stability up to 2300 °C and high thermal stability compared to other ceramic coatings.[36] The elution of the ceramic coated layer on the electrode in this pH range (3.5-12.0) is thought to be negligible.

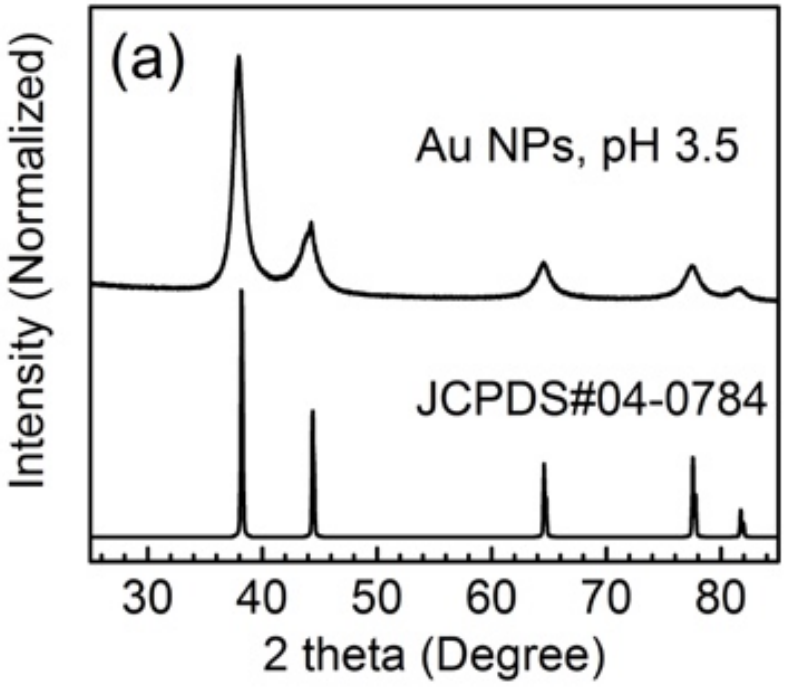

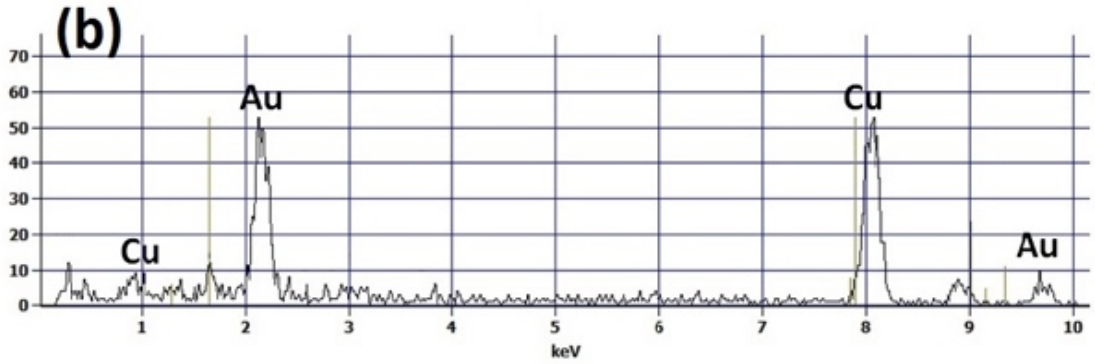

Figure 2.4 (a) XRD pattern and (b) EDS spectrum of Au NPs synthesized in solution pH 3.5. The JCPDS number of XRD reference for cubic Au was indicated.

2.5 Conclusion

In this chapter, ceramic (Y_2O_3)-coated electrode was used in a plasma-in-liquid process (PLP) to create highly pure Au NPs. The high purity was secured by low

erosion and elution rate of the Y_2O_3 coating. The bimodal size distribution of Au NPs was observed for pH in range of 3.5 – 12.0. Small sized (average size 2.1 – 3.1 nm) Au NPs were dominant while large sized ones were considerable at pH = 3.5. A low reduction rate of Au^{3+} ions and non-homogenous NP growth can be taken into account for the bimodal size distribution. As a result, different from the case of PLP by pulse discharge with uncoated electrodes, a strong dependence between pH and particle size was not observed in our case, instead a redistribution of the number of big and small NPs was varied with pH.

2.6 References

1. S. Eustis and M. A. El-Sayed, *Chem. Soc. Rev.,* **2006,** 35, 209.
2. S. Peglow, M. Pohl, A. Kruth and V. Brüser, *J. Phys. Chem. C*, **2015**, 119, 563.
3. N. Toshima and T. Yonezawa, *New J. Chem.,* **1998,** 22, 1179.
4. M. S. Chen and D. W. Goodman, *Acc. Chem. Res.,* **2006**, 39, 739.
5. T. Sumi, S. Motono, Y. Ishida, N. Shirahata and T. Yonezawa, *Langmuir*, **2015**, 31, 4323.
6. T. Yonezawa, H. Tsukamoto and M. Matsubara, *RSC Adv.*, **2015**, 5, 61290.
7. T. Stuchinskaya, M. Moreno, M. J. Cook, D. R. Edwards and D. A. Russell, *Photochem. Photobiol. Sci.*, **2011**, 10, 822.
8. S. D. Brown, P. Nativo, J.-A. Smith, D. Stirling, P. R. Edwards, B. Venugopal, D. J. Flint, J. A. Plumb, D. Graham and N. J. J. Wheate, *J. Am. Chem. Soc.,*

2010, 132, 4678.

9. N. Nath and A. Chilkoti, Anal. Chem., **2002**, 74, 504.
10. S. D. Perrault and W. C. W. Chan, *Proc. Nat. Acad. Sci. USA*, **2010,** 107, 11194.
11. G. Peng, U. Tisch, O. Adams, M. Hakim, N. Shehada, Y. Y. Broza, S. Bilan, R. Abdah-Bortnyak, A. Kuten and H. Haick, *Nature Nanotech.,* **2009**, 4, 669.
12. D. T. Thompson, Nano Today, **2007**, 2, 40.
13. T. Yonezawa, T. Tominaga and D. Richard, *J. Chem. Soc. Dalton Trans.,* **1996,** 883.
14. H. Kawasaki, T. Yao, T. Suganuma, K. Okumura, Y. Iwaki, T. Yonezawa, T. Kikuchi and R. Arakawa, *Chem. Eur.-J.,* **2010,** 16, 10832.
15. Y.-C. Yen, B. Creran and V. M. Rottello, *Nanoscale,* **2012**, 4, 1871.
16. K. Saha, S. S. Agasti, C. Kim, X. Li and V. M. Rottello, *Chem. Rev.,* **2012,** 112, 2739.
17. M. Brust, J. Fink, D. Bethell, D. J. Schiffrin and C. Kiely, *J. Chem. Soc., Chem. Commun.*, **1995,** 1655.
18. B. S. Zelakiewicz, T. Yonezawa and Y. Tong, *J. Am. Chem. Soc.,* **2004**, 126, 8112.
19. V. Amendola, S. Polizzi and M. Meneghetti, *J. Phys. Chem. B,* **2006,** 110,

7232.

20. Y. Shishino, T. Yonezawa, S. Udagawa, K. Hase and H. Nishihara, *Angew. Chem. Int. Ed.,* **2011,** 50, 703.

21. S. Horikoshi and N. Serpone, Eds. In Microwaves in Nanoparticle Synthesis: Fundamentals and Applications, Wiley-VCH Verlag GmbH & Co. KGaA, Weinheim, **2013**, Germany, Chap. 1, 1.

22. S. Sato, K. Mori, O. Ariyada, H. Atsushi and T. Yonezawa, *Surf. Coat. Tech.,* **2011,** 206, 955.

23. M.A. Bratescu, S.-P. Cho, T. Osamu and N. Saito, *J. Phys. Chem. C*, **2011,** 115, 24569.

24. Y. Hattori, S. Mukasa, H. Toyota, T. Inoue and S. Nomura*, Mater. Lett.,* **2011,** 65, 188.

25. H. Lee, S. H. Park, J. J. Kim, Y. K. Park, B. H. Kim and S. C. Jung, *Microelectron. Eng.,* **2015,** 126, 153.

26. Y. Hattori, S. Nomura, S. Mukasa, H. Toyota, T. Inoue and T. Kasahara, J. *Alloys Compd.,* **2013,** 560, 105.

27. Y. Ishida, Y. Motokane, T. Tokunaga and T. Yonezawa, *Phys. Chem. Chem. Phys.,* **2015,** 17, 24556.

28. P. Lukes, M. Clupek, V.Babicky and P. Sunka, *IEEE Trans. Plasma Sci.,* **2008,**

36, 1146.

29. T. Yonezawa, A. Hyono, S. Sato and O. Ariyada, *Chem. Lett.,* **2010**, 39, 783.

30. D. V. Goia and E, Matijevic, *Colloid. Surface. A,* **1999,** 146, 139.

31. X. Ji, X. Song, J. Li, Y. Bai, W. Yang and X. Peng, *J. Am. Chem. Soc.,* **2007**, 129, 13939.

32. S. Biggs, P. Mulvaney, C. F. Zukoski and F. Grieser, *J. Am. Chem. Soc.,* **1994,** 116, 9150.

33. N. Saito, J. Hieda, O. Takai, *Thin Solid Films,* **2009,** 518, 912.

34. G.S. May, C. J. Spanos, *IEEE***, 2006,** 98 , ISBN-10: 0-471-78406-0.

35. D.M. Kim, K.B. Kim, S.Y. Yoon, Y.S. OH, H.T. Kim, S. M. Lee*, J. Ceram. Soc. Jpn.,* **2009,** 117, 863.

36. D. H. Kuo and W. R. Chen*, Thin Solid Films,* **2006,** 497, 65.

3 L-arginine stabilized highly uniform Ag nanoparticles prepared in microwave induced plasma-in-liquid process (MWPLP)

3.1 Introduction

Metallic nanoparticles (NP) and fine particles are of a great interest for their variety of applications, especially their use in printed electronics,[1-4] medicine,[5-11] catalysis[12] and biotechnology.[11,13] Several methods have been used for metallic

NPs preparation, there between the most commonly used are chemical reduction,[14,15] laser ablation[16,17] and plasma sputtering.[18-20] Chemical reduction as the most common method has several disadvantages such as contamination of the particles by reducing agents (alcohol, $NaBH_4$, N_2H_4, citrate, polyol, etc.), and their following complicated purification process. In contrast microwave plasma in liquid process (MWPLP) represents green alternative in a NP synthesis field due to its relatively low energy consumption and no necessity to use toxic reducing agents. This is because plasma generated under reduced pressure decomposes water molecules to form highly reactive species, e.g. solvated electron (e^-_{aq}) and hydrogen (H•) radicals, which can reduce metal ions, M^{n+}.[21,22] The reduction of metal ions by reactive species formed in plasma discharge can occur as follows:

$M^{n+} + nH\bullet \rightarrow M^0 + nH^+$

$M^{n+} + ne^-_{aq} \rightarrow M^0$

at low pH or via below reaction:

$M^{n+} + ne^-_{aq} \rightarrow M^0$

at high pH.

As a result, this approach has been used for preparation of various metallic NPs such as Ag, Au, Pt, Zn, Sn.[23-28] As a recent progress, our research group has

introduced the use of ceramic (Y_2O_3)-coated electrode for synthesizing pure metal NPs[21,23,28] to eliminate impurities emitted from the conventionally used tungsten electrode.[24,29] Consequently, we have demonstrated that pure Au and Ag NPs were successfully prepared with addition of H_2O_2 as a reducing additive using coated electrode for the first time.[21,28]

As silver NPs are widely used for their high extinction, antibacterial and biocompatible properties, and low cost compared with other noble metal NPs, synthesis of pure Ag NPs also received great attention. However, in comparison with Au or Pt NPs, single size Ag NPs are more challenging to achieve. This is caused by incomplete reduction of silver ions even though excessive reducing agent was used, meaning that secondary nucleation and growth occur during the reaction course, which results to a broad size distribution of Ag NPs.[30,31] Besides, it is known that the uniformity, size and shape of the Ag NPs used in certain applications especially medicine can be crucial for their resulting effect for desired use.[11,30] For example, smaller Ag NPs display higher antimicrobial activity[30,32] and truncated-triangular NPs are believed to be more effective for microbial killing.[33]

While microwave induced plasma in liquid using coated electrode can offer a green synthesis method for pure Ag NPs, a strategy to tailor particle size with

good uniformity is highly demanded. So far, the reduction of metal ions in MWPLP using a coated electrode is relatively low,[21,23,28] and a nonhomogeneous reaction often causes the formation of polydispersed NPs. Thus, we need to establish conditions for a higher reduction speed under microwave-induced plasma in liquid using coated electrode and to add a suitable stabilizing agent for control of particle growth and to prevent their aggregation.[34,35] The pH adjustment can be a very powerful tool in this case.[23,25,28] Our previous study with coated electrode suggested varying the pH of reaction solution, i.e. pH = 3.5 – 12, can change the reduction speed of metal ion precursors and the size dispersion of the obtained Au and Ag NPs.[25,28] In particular pH 12 allowed to synthesize Au NPs with smaller size and narrower size distribution compared with NPs obtained using lower pH. However, at high pH the commonly used $AgNO_3$ precursor is converted to silver hydroxide and then to silver oxides, this makes the reduction, nucleation and growth of Ag NPs from these precursors more difficult to control. Hence, to prevent such un-desired phenomenon to occur when increasing pH, we proposed a strategy based on the use of a high pH stable and water-soluble silver complex, i.e. $Ag[NH_3]_2^+$ in the synthesis of Ag NPs.[28] The use of this complex is advantageous as it is water soluble complex for uniform growth of silver NPs and can be prepared simply by adding ammonia solution to $AgNO_3$ whereas ammonia

solution can be used in pH adjustment. In the previous report,[28] the reduction of silver complex was obtained via plasma and H_2O_2 reduction whereas the size dependent pH was studied in the absence of a capping ligand. In our present synthesis strategy, we choose L-arginine as the stabilizing agent for Ag NPs produced under plasma discharge. This is because L-arginine is a natural amino acid, which is non-toxic and has good biocompatibility and available functional groups for binding with Ag NP surface to stabilize them as it was previously used in the chemical synthesis of Ag NPs.[36] We have demonstrated that our synthesis approach using $Ag[NH_3]_2^+$ complex and L-arginine as the stabilizing agent without addition of a reducing agent allowed us to control particle size with high uniformity and to attain small sized, of ca. 5 nm, and pure Ag NPs.

3.2 Aim of this chapter

In previous chapter, we have introduced yttrium oxide (Y_2O_3) coated stainless steel electrode to challenge impurity problems of resulting NPs due to the loss of electrode materials. In this chapter, we proposed using $[Ag(NH_3)_2]^+$ complex as the alternative precursor and L-arginine as the stabilizing agent to synthesize highly uniform Ag NPs with an average diameter of around 5 nm. $[Ag(NH_3)_2]^+$ complex was chosen as it can allow the reaction proceed at high pH for higher reaction yield compared with using $AgNO_3$ whereas L-arginine can stabilize Ag NPs to attain highly uniform and small sizes. The influence of the selection of

initial precursor on the reduction of metal precursor during the plasma irradiation, the particle size and size distribution of Ag NPs, and influence of the amount of L-arginine, were investigated.

3.3 Experimental

3.3.1 Apparatus

The schematic illustration of solution plasma reactor is shown in Figure 3.1a.[23,28] Microwaves (2.45 GHz) are emitted from magnetron (Micro-denshi UW-1500) and pass through a WRJ-2 rectangular waveguide (109.22 × 54.61 mm^2), a power meter, a tuner, a waveguide to the coaxial adaptor, and plasma source. The coaxial electrode is attached in the middle of waveguide and her front is projected in to the chamber. This coaxial electrode is ended by an Y_2O_3-coated stainless steel sharp tip (Figure 3.1b). The stainless-steel reactor (500 cm^3) is coated inside with PTFE. Plasma solution is cooled by a stainless cooling spiral with chilled liquid at 5 °C. Plasma ignition and the solution during plasma reaction can be observed by eye through the quartz window. Pressure was decreased by a diaphragm vacuum pump and measured by a vacuum gauge.

3.3.2 Materials

Silver nitrate ($AgNO_3$, min. 99.8%, Junsei, Japan) and L-arginine ($C_6H_{14}N_4O_2$, Junsei) were used as a precursor and a stabilizer, respectively. Ammonia solution (NH_3, min. 28%, GR, Junsei), was used for pH adjustment to pH 11.0 and to form silver diamine complex ($[Ag(NH_3)_2]^+$) as the alternate precursor. Potassium iodide (KI, Kanto, Japan) was used for observation of unreacted Ag^+ ions in the solution during the plasma reaction at various times (0, 5, 10, 20, 60, 100, 140 min) and thus also their reduction speed.[28] All chemicals were used as received. The deionized water (Organo/ELGA purelabo system, > 18.2 MΩ·cm) was used to prepare solution for plasma reaction.

3.3.3 Synthesis of Ag NPs

2.12 cm^3 of aqueous $AgNO_3$ (0.12 M) was added into 500 cm^3 of water to obtain $AgNO_3$ concentration of 0.5 mM, followed by the addition of aqueous L-arginine (0.287 M) in various amount (0.087, 1.74, 8.7 cm^3). The molar ratio of Ag complex and L-arginine was 1:0.1, 1:2, and 1:10, respectively. The solution pH was adjusted to pH 11.0 by addition of ammonia solution. The mixed solution was stirred for 10 minutes, and then introduced into the reaction vessel. The plasma was initiated at 450 W of the microwave output. Then, in order to keep plasma generation, the output was kept at 400 W during whole reaction. The plasma reaction was conducted for 140 min.

3.3.4 Characterization

UV-Vis spectra were collected in order to observe Ag NPs formation at different time and pH using an UV-Vis spectrophotometer (Shimadzu UV-1800) and a quartz cell with 1 cm optical path. During plasma reaction, 3 cm^3 of the sample solutions were taken directly from the plasma chamber for each measurement at various reaction time. After 140 min plasma discharge, reaction solutions were purified by means of dialysis then evaporated to half of the volume for taking UV-Vis spectra. The dispersion of Ag NPs prepared using diamine complex without L-arginine was dialyzed and used for collecting UV-Vis spectrum without any further treatment. A part of the dialyzed samples was completely evaporated, and powder was used to analyze with Fourier transform infrared spectroscopy (FT-IR, FT/IR-4600, Jasco) to investigate stabilizing effect of L-arginine on Ag NPs.

The transmission electron microscopy (TEM, JEOL JEM 2000-ES, at 200 kV) with an energy dispersive X-ray spectroscope (EDS) was used to analyze the morphology, elemental composition and Ag NPs formation in time. Ag NP solutions were at first purified by membrane dialysis for 3 days, and then the purified solution was dropped on collodion film-coated copper TEM grids, and naturally dried. From 100 to 150 NPs were used to estimate the particle size, in arbitrary chosen areas, and size distribution using TEM images. A part of the NPs solutions was filtrated through 0.1 μm mixed cellulose filter and examined with X-

ray diffraction (XRD, Rigaku MiniFlex II, Cu Kα radiation, scanning rate of 5 ° min^{-1}). Thermogravimetric-differential thermal analysis (TG-DTA) was performed on a Shimadzu DTG-60H using 3% H_2/N_2 gas with heating rate of 5 °C min^{-1} from 25 to 700 °C. L-arginine stabilized Ag NPs were filtered (0.1 μm pore size membrane) and washed with water, then the powder was collected and dried before TG-DTA analysis. Part of the dispersion obtained after 140 min plasma discharge was used for measuring Zeta potential using the Photal Otsuka Electronics- ELSZ-2NMP.

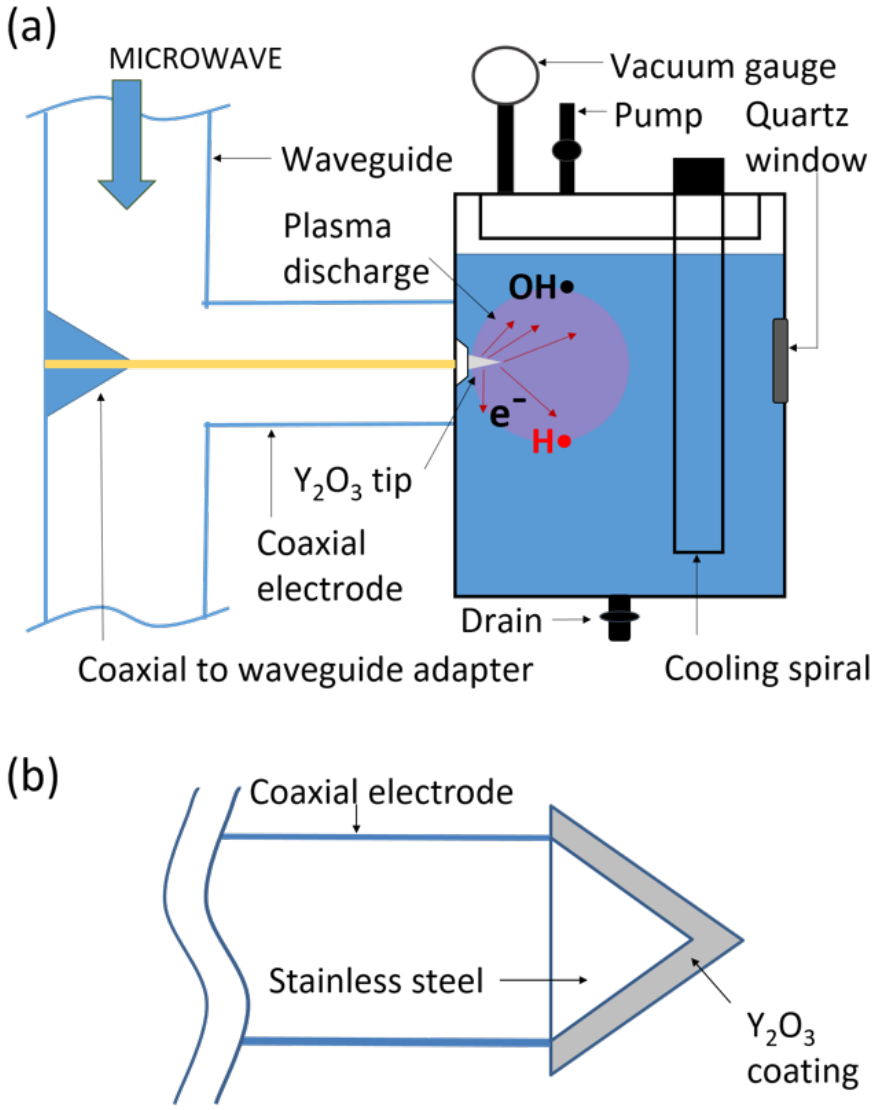

Figure 3.1 (a) Schematic illustration of the plasma reactor of microwave induced plasma-in-liquid process used in this study and (b) configuration of the Y_2O_3-coated stainless steel electrode.

3.4 Results and Discussion

3.4.1 Ag nanoparticles formed using $AgNO_3$ and $[Ag(NH_3)_2]^+$ complex as metal precursors

Commonly used silver nitrate ($AgNO_3$) as a metal precursor in acidic pH for synthesis of Ag NPs shows that Ag ions are not reduced completely in chemical reduction. Non-robust reduction of Ag^+ ions and growth of Ag NPs causes interference between nucleation and growth which in turn often results into large size distribution with difficulties in size control. In our study, we found similar phenomenon while using silver nitrate as the metal precursor in MWPLP. As shown in Figure 3.2a and inset of Figure 3.2a, MWPLP produced Ag NPs of bimodal size with two fractions of 8.3 ± 1.4 nm and 88.4 ± 25.3 nm. Size of the bigger fraction of the Ag NPs is similar to that prepared in citrate method by Pillai et al. (particle size diameter between 50-100 nm)[37], while the size of the smaller fraction of the NPs is similar to that prepared by MWPLP using uncoated tungsten electrode.[24] S. Sato at al. reported rapid formation of Ag NPs in just 90 s of plasma irradiation with the obtained NP size ca. 4.5 nm, however tungsten was vaporized from the electrode by plasma, and could cause contamination of the produced NPs. Use of Y_2O_3 coated electrode tip can prevent such a phenomenon due to

the low elution and erosion rate of the Y_2O_3 coating. On the other hand, use of ceramic-coated electrode tip caused slower reduction of the Ag ions and bimodal distribution of the obtained NPs.

In order to eliminate bimodal size distribution and to use a silver molecular precursor in basic pH we suggested addition of ammonia to the silver nitrate solution. This simple method allow us to form homogenous and water soluble silver diamine complex ($[Ag(NH_3)_2]^+$) at high pH as in the following equation:

$$Ag^+_{(aq)} + 2NH_{3(aq)} \rightarrow [Ag(NH_3)_2]^+_{(aq)} \qquad (1)$$

Using $[Ag(NH_3)_2]^+$complex as silver precursor (Figure 3.2b) under the same conditions as using silver nitrate (Figure 3.2a), Ag NPs with narrower size distribution (128.7 ± 18.9 nm) were obtained (Figures 3.2c and 3.2d). Similar particle sizes and size distributions were also found when H_2O_2 was used as a reducing additive.[28] At pH = 11, the average particle sizes are 150 ($[H_2O_2]$ = 0.0015 mM) – 400 ($[H_2O_2]$ = 0.075 mM) nm which were varied with the concentration of H_2O_2. This is consistent with the higher reduction speed of silver diamine complex compared with that of silver nitrate (Figure 3.2f), because higher reduction speed allows for more robust nucleation and NP growth. The absorption peak areas of AgI used for estimation of the reduction speed and preparation of Figure 3.2f are showed in Figure 3.3.

The position and intensity of the localized surface plasmon resonance (LSPR) peak for Ag NPs can vary regarding to the size and aggregation of Ag NPs. The

UV-Vis spectrum of the sample prepared from $[Ag(NH_3)_2]^+$ complex shows a wide absorbance LSPR band at high wavelength, *i.e.*, 450 – 600 nm. This is attributed to the longitudinal LSPR caused by the plate-like structure of these resulting Ag NPs as also reported elsewhere.[38] A valley near 320 nm was observed which is possibly caused by an overlapping of the absorption at around 290 nm for Ag clusters and the broad LSPR peak of disc-shaped Ag NPs. The particle size of Ag NPs produced from silver diamine complex is quite big. This indicated that the growth of Ag NPs continued to occur during plasma irradiation and excess ammonia or hydroxyl ions did not effectively protect Ag NPs. Therefore, in order to reduce the particle size, L-arginine as the protecting agent was introduced to the reaction solution.

3.4.2 Ag nanoparticles formed using various amount of L-Arginine

L-arginine is one of the non-toxic, biocompatible amino acids used in the biosynthesis of proteins. In this part of the study, we have used L-arginine to stabilize Ag NPs and prevent the growth of Ag NPs during plasma discharge to obtain small Ag NPs with narrow size distribution. L-arginine was added to the reaction solution with molar ratio of $[Ag(NH_3)_2]^+$ to L-arginine, hereafter Ag : Arg, of 1 : 0.1, 1 : 2, and 1 : 10. As shown in Figure 3.4a, when small amount of L-arginine was used (Ag : Arg = 1 : 0.1 (mol/mol)), beside small Ag NPs (5.0 ± 0.5 nm) some big Ag NPs (235.6 ± 25.6 nm) were still observed. This was also

confirmed by UV-vis spectrum of this sample shown in Figure 3.5. Beside transverse LSPR band at 420 nm for Ag NPs, the longitudinal characteristic absorbance band in 450 – 600 nm were observed for plate-like Ag NPs.[30,39,40] These big plate-like Ag NPs are similar as one obtained without using of L-arginine (Figure 3.2b). On the other hand, an increase in the amount of L-arginine (Ag : Arg = 1 : 2 and 1 : 10 (mol/mol)) resulted in small, single sized Ag NPs (5.5 ± 0.6 nm and 5.1± 0.7 nm, respectively), without any big Ag NPs formed (Figures 3.4b and c). UV-Vis spectra (Figure 3.5) for these samples showed a peak at around 430 nm without the broad absorbance band at higher wavelength as observed for plate-like Ag NPs. This indicated the formation of spherical Ag NPs and complete absence of plate-like Ag NPs. The XRD result (Figure 3.6) of resulting NPs obtained using Ag : Arg = 1 : 2 molar ratio further confirmed that our obtained NPs are metallic Ag.

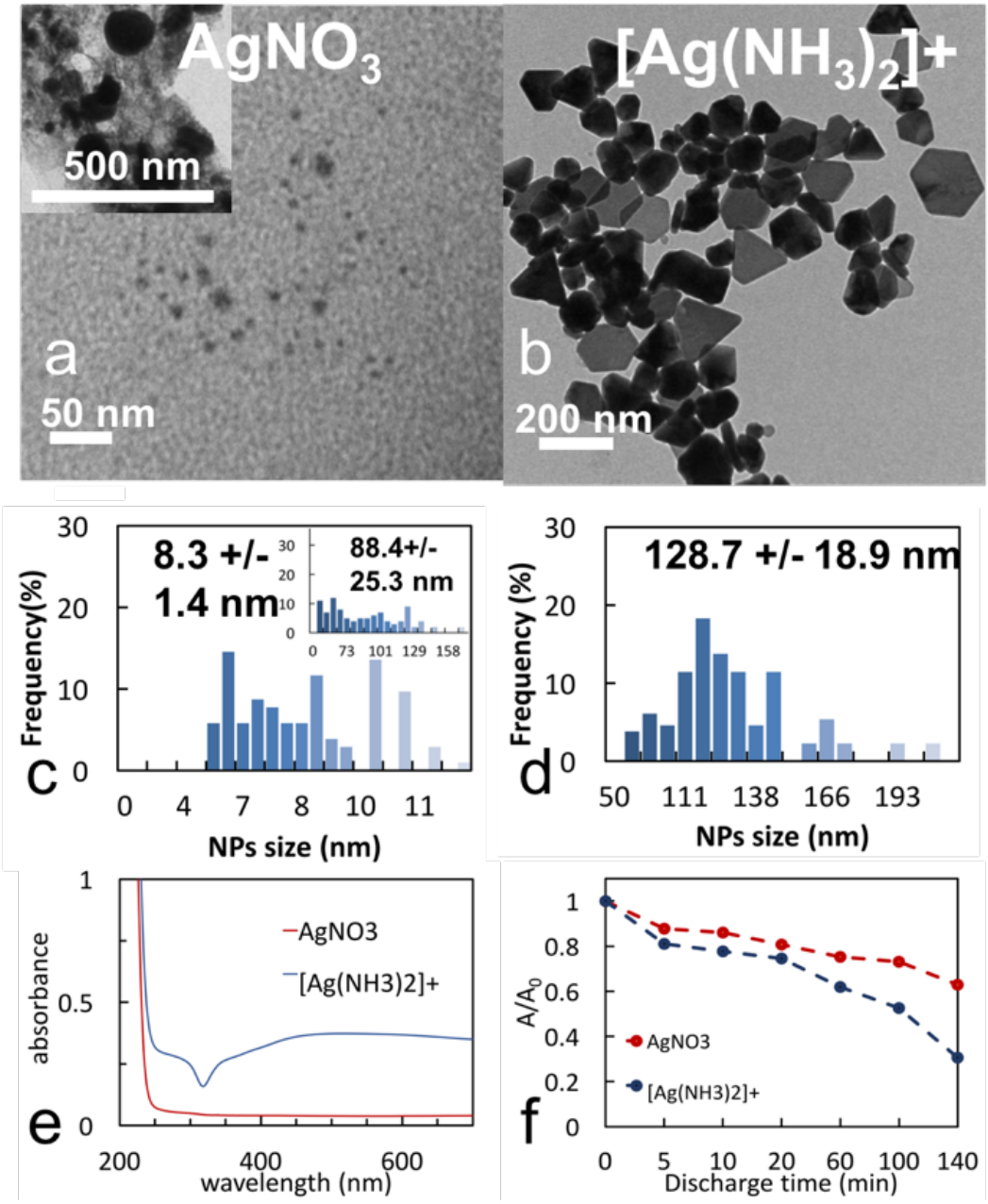

Figure 3.2 (a) TEM image and (c) size distribution of Ag NPs prepared using silver nitrate as metal precursor, (b) TEM image and (d) size distribution of Ag NPs prepared using silver diamine complex as metal precursor, (e) UV-Vis spectra of Ag NPs prepared using $AgNO_3$ and $[Ag(NH_3)_2]^+$ complex (f) reduction speed monitored via plot of A/A_0 as function of reaction time where A is the peak

area of the absorption of AgI at ca. 420 nm during plasma discharge and A_0 is the peak area of the absorption of AgI at ca. 420 nm before plasma irradiation shown in Figure 3.3.

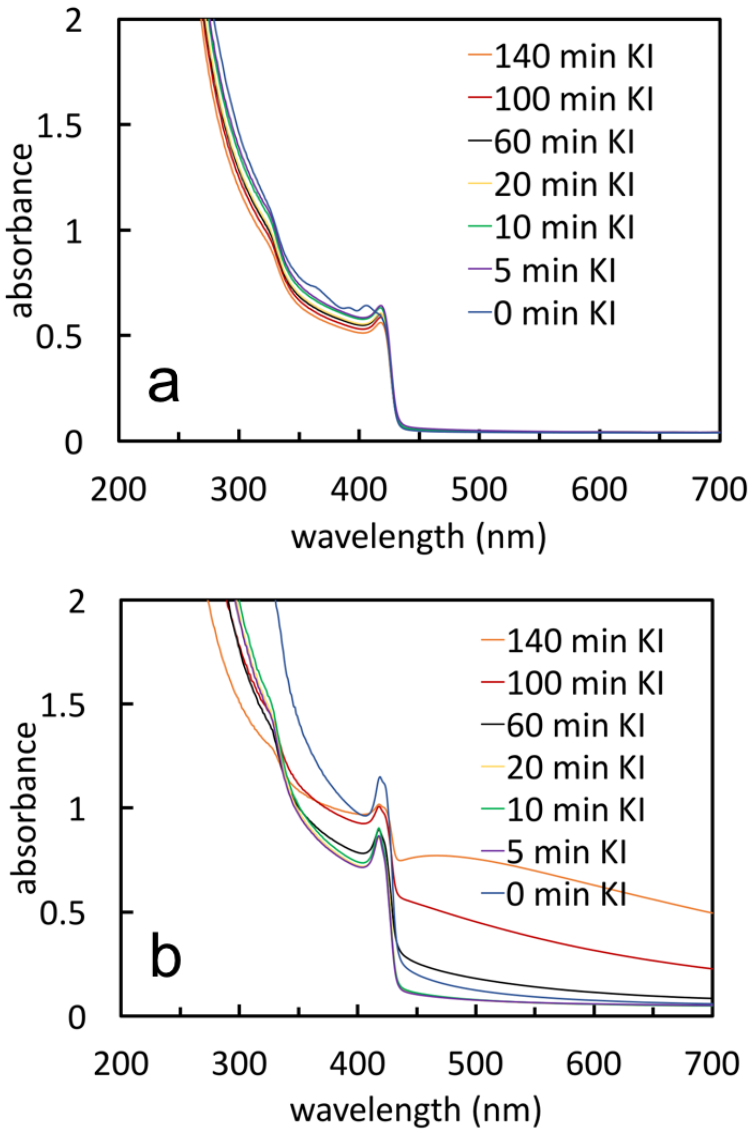

Figure 3.3 (a,b) Time dependent UV-Vis spectra observation of AgI at ca. 420 nm, formed by addition of KI into the taken out samples, during preparation of Ag NPs with: a) $AgNO_3$, b) $[Ag(NH_3)_2]^+$ as the precursors.

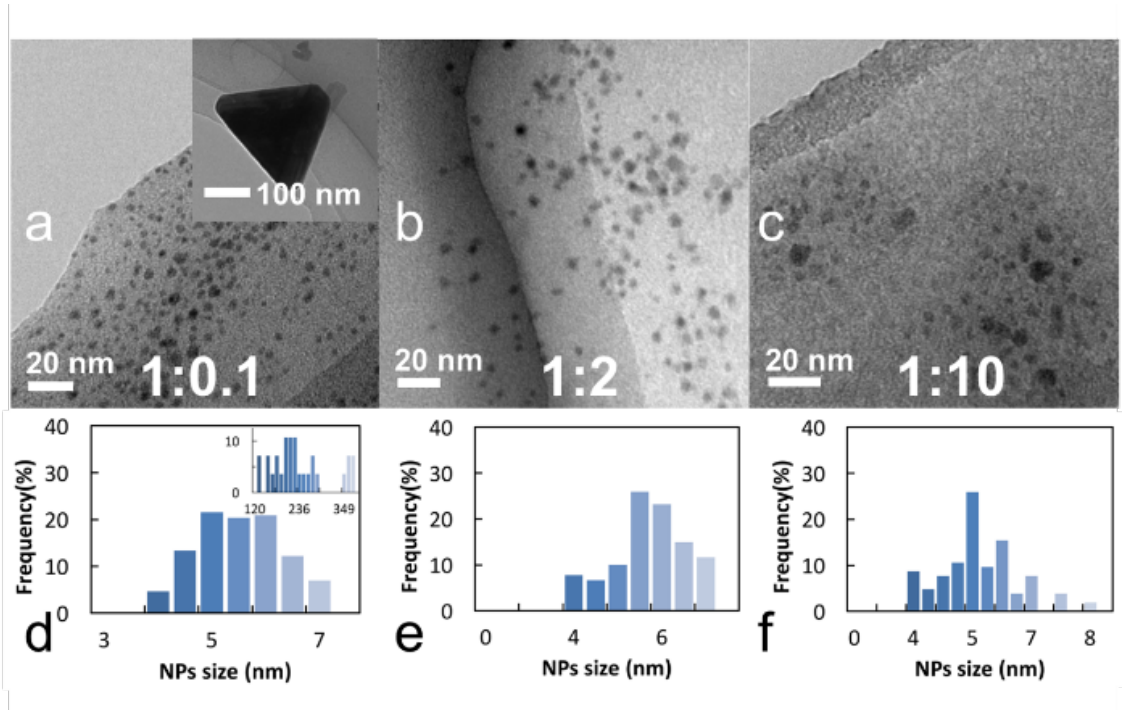

Figure 3.4 TEM image and size distribution of Ag NPs obtained using molar ratio of $[Ag(NH_3)_2]^+$ to L-arginine (Ag : Arg) of (a, d) 1 : 0.1, (b, e) 1 : 2 and (c, f) 1 : 10 .

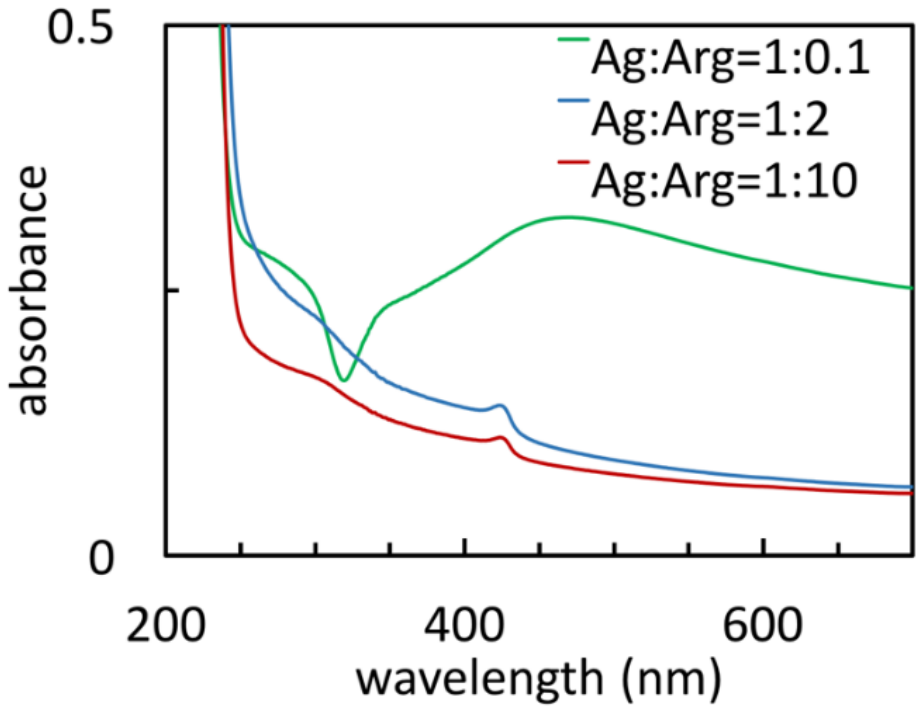

Figure 3.5 UV-Vis spectra of Ag NPs obtained using Ag : Arg molar ratios of 1 : 0.1 (green curve), 1 : 2 (blue curve), and 1 : 10 (red curve).

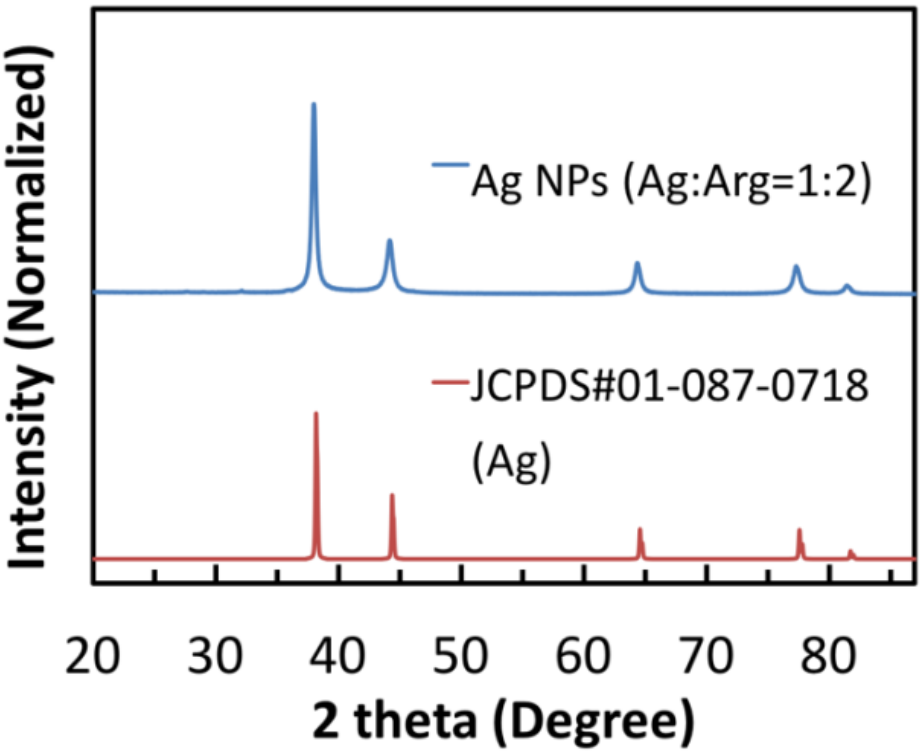

Figure 3.6 XRD pattern of Ag NPs synthesized using a molar ratio of silver complex to L-arginine of 1:2.

Table 3.1 Average diameter of Ag NPs prepared with silver diamine complex ($[Ag(NH_3)_2]^+$) as the precursor with various ratios of silver complex and L-arginine.

Ag:Arg (mol/mol)	**1:0**	**1:0.1**	**1:2**	**1:10**
NP size (nm)	128.7 ± 18.9	5.0 ± 0.5	5.5 ± 0.6	5.1 ± 0.7

Table 3.1 shows average diameter of Ag NPs prepared without and with L-arginine as the stabilizing agent with different ratio of Ag : Arg (mol/mol). As it is clearly visible from the particles size change tendency, over the certain amount,

i.e. Ag:Arg 1:2 (mol/mol), L-arginine can effectively stabilize Ag NPs and prevent their further growth, and in combination with access of NH_3, which forms $[Ag(NH_3)_2]^+$ complex, limit the secondary nucleation step and avoid bimodal size distribution.

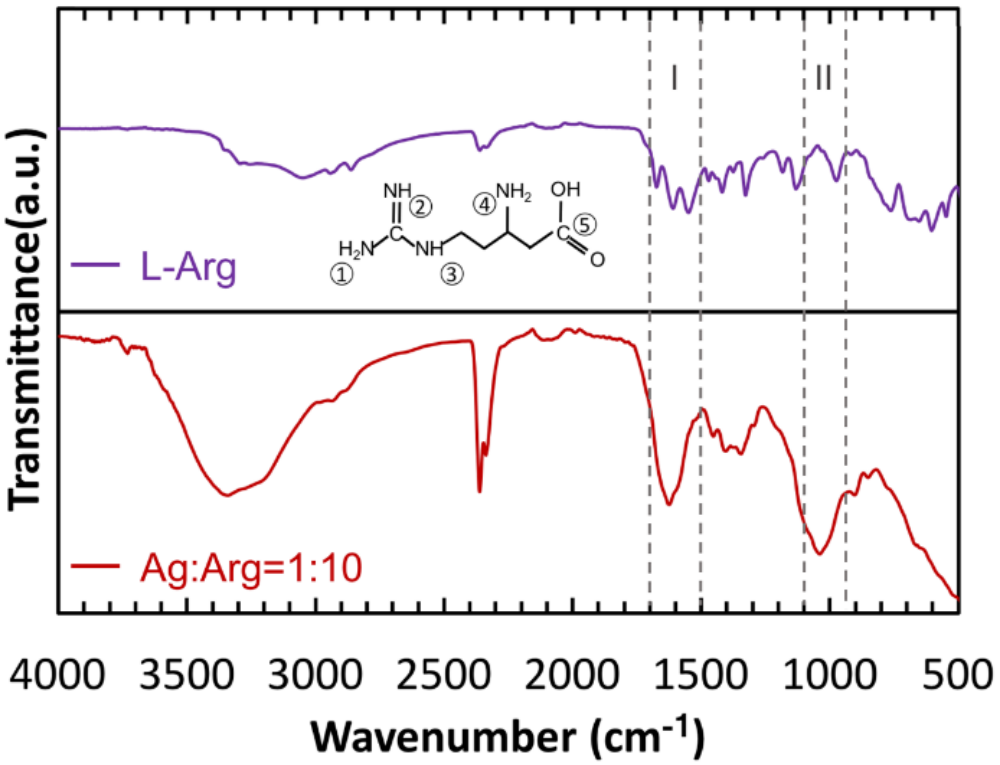

Figure 3.7 FT-IR of L-arginine, Ag NPs stabilized with L-arginine, and Ag NPs prepared using $AgNO_3$.

Table 3.2 FT-IR peak assignment for main peaks in FT-IR spectra in Figure 3.7

Peak position (cm^{-1})	Pure L-arginine	Ag:Arg = 1:10
O-H, stretch, water	N/A	3200-3400
N-H, stretch (group 3)	3352	3352
O-H stretch (group 5)	3297	3297
O=C=O (in air)	2353	2353
C=O stretch, carboxylic acid (group 5)	1673	Overlap with C=N
C=N, stretch (group 2)	1613	1627
N-H, bend (group 1, 4)	1551	1593
O-H bending, carboxylic acid (group 5)	977	1038

To understand the binding of L-arginine and particle surface, we collected the FT-IR spectra of Ag NPs stabilized with L-arginine (Ag:Arg = 1 : 10 (mol/mol)) and pure L-arginine.

The peak assignment is given in Table 3.2 in details. The L–arginine showed its characteristic bands at 3352 cm^{-1} for N-H stretch in secondary amines, 3297 cm^{-1} for O-H stretch, 1673 cm^{-1} for C=O stretch for carboxylic acid, 1613 cm^{-1} for C=N stretch, 1551 cm^{-1} for N-H bend of primary amines, 977 cm^{-1} for O-H bend in carboxylic acid[36,41]. In case of L-arginine capped Ag NPs prepared using Ag:Arg 1:10 (mol/mol), we detected the characteristic vibrations of L-arginine as shown in Table 3.2. This confirms that the organic capping agent exists on the surface of the obtained Ag NPs. Moreover, it was observed that the peak for N-

H stretch was shifted to the higher wave number (Δ = 42 cm^{-1}) whereas the peak for O-H stretch in carboxylic group is significantly shifted to the higher wave number (Δ = 61 cm^{-1}) compared with pure L-arginine. These shifts can be caused via binding of L-arginine to particle surface and the change in the form of L-arginine at high pH. At a pH, *i.e.* 11, higher than the isoelectric point of L-arginine, *i.e.* p_I=10.76, L-arginine is protonated to form COO^- and α amine group (group 4) becomes NH_3^+. The zeta potential of the resulting Ag colloidal solution is of -32 mV (Ag : Arg = 1:10), which suggested that particles had negative charge and were colloidal stable in the solution. Zeta potential of Ag NP dispersion prepared with different silver precursor to L-arginine ratios also indicated negative surface charge of Ag NPs. It was noticed that the change in Zeta potential did not simply follow the increase in ratio of L-arginine used. Zeta potential of -31 mV and -13 mV was found in dispersion prepared with Ag : Arg = 1:0.1 and 1:2 (mol/mol), respectively. Relatively high absolute value of Zeta potential when the least L-arginine was used can relate to the anisotropic shape and big size of the plate-like Ag NPs as reported elsewhere.[42,43] Even though the sample prepared with the least L-arginine has relatively high absolute value of Zeta potential, it is not as stable as others. We observed that precipitation occurred in the dispersion of Ag NPs prepared with Ag : Arg = 1:0.1 (mol/mol) after 24 h (least L-arginine)

whereas Ag NP dispersions prepared using Ag : Arg = 1:2 and 1:10 (mol/mol) were stable after 2 weeks (Figure 3.8). This can be attributed to the precipitation of the big size Ag NPs which may require much higher Zeta potential value to stabilize them.[42.43] Besides, TG analysis of the obtained L-arginine stabilized Ag NPs prepared using Ag : Arg = 1:10 (mol/mol) under 3% H_2/N_2 (Figure 3.9) indicated that there was significant weight loss, i.e. 49.75 % when temperature increases from 160 °C to 600 °C. Corresponding to this weight loss, there was an endothermic peak centre at 400 °C, which belongs to the evaporation of L-arginine (boiling point of 368 °C) from the Ag particle surface. The small weight loss below 160 °C is due to the absorbed water. When the initial molar ratio of silver precursor to L-arginine of 1:0.1, there was just 6.6 % of the weight loss attributed to L-arginine (Figure 3.10). This result further indicated that the smaller size Ag NPs were well capped with L-arginine.

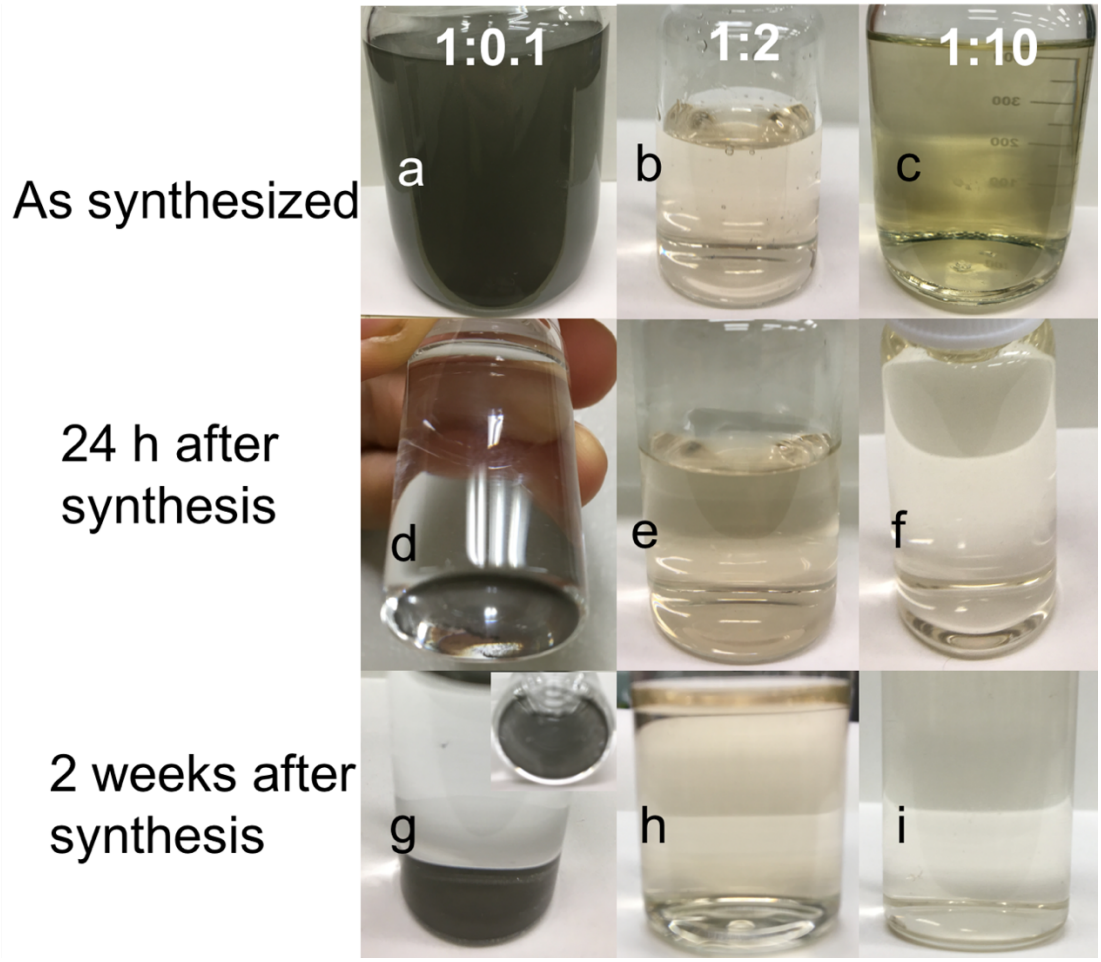

Figure 3.8 Photographs of the obtained dispersions of L-arginine stabilized Ag NPs synthesized using different ratios of Ag precursor and L-arginine 1:0.1, 1:2, 1:10 mol/mol: (a-c) as-synthesized, (b-f) 24 h after synthesis, (g-h) 2 weeks after synthesis.

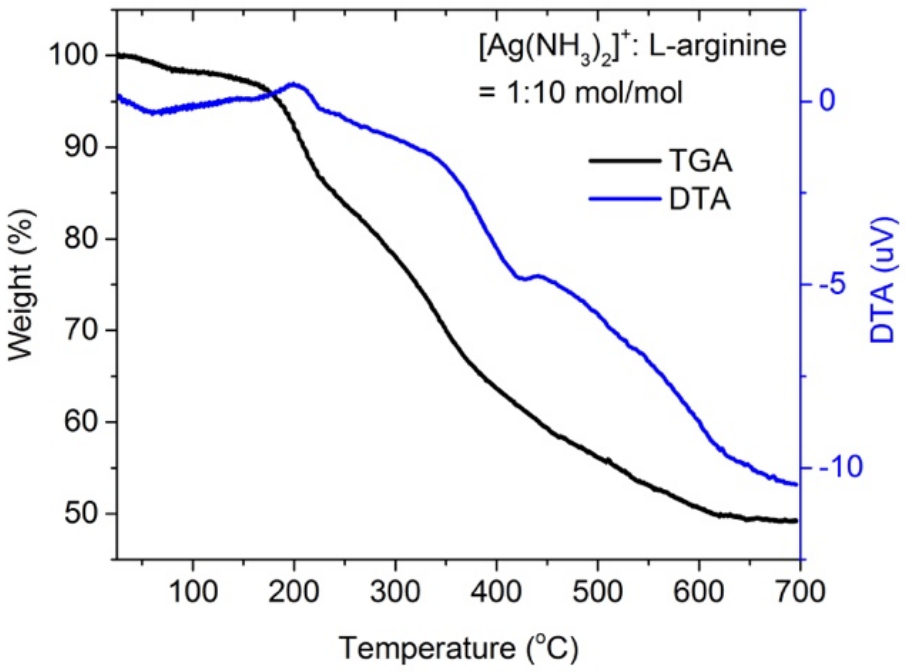

Figure 3.9 TG-DTA curve for L-arginine capped Ag NPs prepared using Ag : Arg = 1:10 (mol/mol).

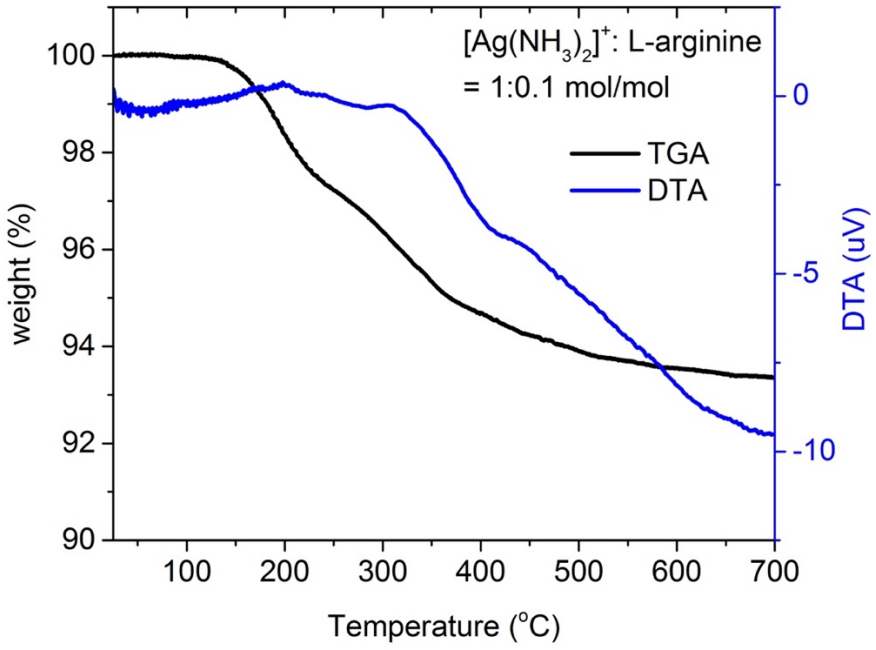

Figure 3.10 TG-DTA curve for L-arginine capped Ag NPs prepared using $[Ag(NH_3)_2]^+$ to L-arginine molar ratio of 1:0.1 (mol/mol).

Based on the shifts in FT-IR spectrum and the possible binding of L-arginine to Ag surface, we suggest that carboxylate group binds to the particles surface to stabilize them as shown in Figure 3.11. F. Wu *et al.*[36] previously also reported that L-arginine can effectively stabilized Ag NPs prepared using silver nitrate as the precursor.

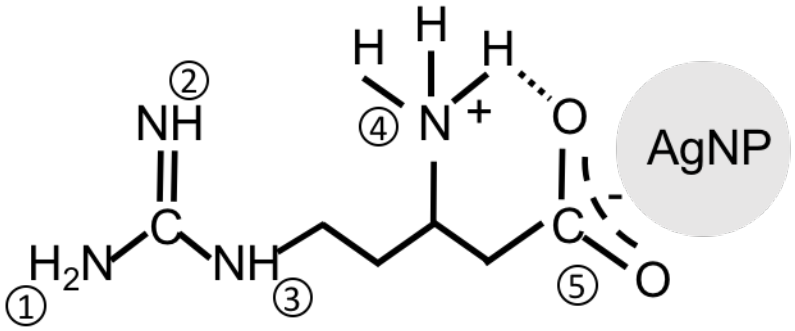

Figure 3.11 Proposed bonding between carboxylate group and silver NPs (particle size and bonding length are not in scale).

The method described in this paper can offer a green approach to synthesize and stabilize metal NPs. Besides L-arginine, other amino acids can be used to prepare Ag NPs. As shown in Figure S4, when L-leucine was used to replace L-arginine ($[Ag(NH_3)_2]^+$: L-leucine = 1:10 (mol/mol)), Ag NPs with average diameter of 9.9±3.3 nm were produced, which means bigger size and wider size distribution compared with L-arginine capped Ag NPs prepared under similar conditions. However, to understand the influence of different amino acids and

other types of capping agents used to control the particle size and uniformity, it is necessary to study more in depth.

3.5 Conclusion

In this chapter, the influence of silver diamine complex as the precursor and L-arginine as a stabilizing agent on the formation of Ag NPs synthesized in MWPLP using a coated electrode was investigated. As a result, a strong influence of L-arginine on NP size, and of silver diamine complex on the uniformity of the synthesized Ag NPs was observed. In conclusion, uniform, small sized (with the average diameter ca. 5 nm) and highly pure Ag NPs can be obtained by addition of silver diamine and L-arginine during MWPLP. The obtained Ag NPs were effectively stabilized by carboxylate group contributed by L-arginine as was confirmed by FT-IR.

3.6 References

37. K. Ankireddy, S. Vunnam, J. Kellar, W. *J. Mater. Chem. C*, **2013**, *1*, 572.

38. D. V. Talapin, J. S. Lee, M. V. Kovalenko, E. V. Shevchenko, *Chem. Rev.*, **2010**, *110*, 389.

39. J. S. Kang, H. S. Kim, J. Ryu, H. T. Hahn, S. Jang, J. W. Joung, *J. Mater. Sci. Mater. Electron.*, **2010**, *21*, 1213.

40. T. Yonezawa, S. Takeoka, H. Kishi, K. Ida, M. Tomonari, *Nanotechnology*, **2008**, *19*, 145706.

41. S. Kim, Y. T. Lim, E. G. Soltesz, A. M. De Grand, J. Lee, A. Nakayama, J.A. Parker, T. Mihaljevic, R. G. Laurence, D. M. Dor, L. H. Cohn, M. G. Bawendi, J. V. Frangioni, *Nat. Biotechnol.*, **2004**, *22*, 93.

42. M. G. Harisinghani, J. Barentsz, P. F. Hahn, W. M. Deserno, S. Tabatabaei, C. H. van de Kaa, J. de la Rosette, R. Weissleder, *New Engl. J. Med.*, **2003***,* 348, 2491.

43. S. Mohanty, S. Mishra, P. Jena, B. Jacob, B. Sarkar, A. Sonawa, *Nanomedicine: NBM*, **2012**, *8*, 916.

44. K. H. L. Kwan, X. L. Liu, M. K. T. To, K. W. K. Yeung, C. M. Ho, K. K. Y. Wong, *Nanomedicine NBM*, **2011**, *7*, 497.

45. C. Tse, M. J. Zohdy, J. Y. Ye, M. O'Donnell, W. Lesniak, L. Balogh, *Nanomedicine: NBM*, **2011**, *7*, 97.

46. E. C. Dreaden, L. A. Austin, M. A. Mackey, M. A. El-Sayed, *Ther. Deliv.*, **2012**, *3*, 457.

47. M. Rai, A. Ydav, A. Gade, *Biotechnol. Adv.*, **2009**, *27*, 76.

48. T. Yonezawa, T. Tominaga, D. Richard, *J. Chem. Soc., Dalton Trans.*, **1996**, 783.

49. P. Tartaj, M. P. Morales, T. Gonzalez-Carreno, S. Veintemillas-Verdaguer, C. J. Serna, *J. Magn. Magn. Mater.*, **2005**, *290-291*, 28.

50. J. Liu, X. Li, X. Zeng, *J. Alloy. Compd.*, **2010**, *494*, 84.

51. Z. Khan, S. A. Al-Thabaiti, A. Y. Obaid, A. O. Al-Youbi, *Colloids Surf. B*, **2011**, *82*, 513.

52. V. Amendola, S. Polizzi, M. Meneghetti, *J. Phys Chem. B*, **2006**, *110*, 7232.

53. N. Haustrup, G. M. O'Connor, *Phys. Procedia*, **2011**, *12*, 46.

54. Y. Ishida, R. Nakabayashi, R. D. Corpuz, T. Yonezawa, *Colloids Surf. A*, **2017**, *518*, 25.

55. M. Porta, M. T. Nguyen, T. Tokunaga, Y. Ishida, W. Liu, T. Yonezawa, *Langmuir*, **2016**, *32*, 12159.

56. Y. Shishino, T. Yonezawa, S. Udagwawa, K. Hase, H. Nishihara, *Angew. Chem. Int. Ed.*, **2011**, *50*, 703.

57. M. Nishimoto, T. Yonezawa, D. Čempel, M. T. Nguyen, Y. Ishida, H. Tsukamoto, *Mater. Chem. Phys.*, **2017**, *193*, 7.

58. T. Ishijima, H. Hotta, H. Sugai, M. Sato, *Appl. Phys. Lett.*, **2007**, *91*, 121501.

59. D. Čempel, M. T. Nguyen, Y. Ishida, Y. Wang, K.C.-W. Wu, T. Yonezawa, *J.*

Nanosci. Nanotechnol., **2016**, *16*, 9257.

60. S. Sato, K. Mori, O. Ariyada, A. Hyono, T. Yonezawa, *Surf. Coat. Tech.*, **2011**, *206*, 955.
61. M. A. Bratescu, S.-P. Cho, O. Takai, N. Saito, *J. Phys. Chem. C*, **2011**, *115*, 24569.
62. Y. Hattori, S. Mukasa, H. Toyota, T. Inoue, S. Nomura, *Mater. Lett.*, **2011**, *65*, 188.
63. H. Lee, S. H. Park, J. J. Kim, Y. K. Park, B. H. Kim, S. C. Jung, *Microelectron. Eng.*, **2015**, *126*, 153.
64. M. Nishimoto, H. Tsukamoto, M. T. Nguyen, T. Yonezawa, *ChemistrySelect*, **2017**, *2*, 7873.
65. Y. Ishida, Y. Motokane, T. Tokunaga and T. Yonezawa, *Phys. Chem. Chem. Phys.*, **2015**, *17*, 24556.
66. S. Agnihotri, S. Mukherjiabc, S. Mukherji, *RSC Adv.*, **2014**, *4*, 3974.
67. L. F. Gorup, E. Longo, E.R. Leite, E. R. Camargo, *J. Colloid Interface Sci.*, **2011**, *360*, 355.
68. J. R. Morones, J. L. Elechiguerra, A. Camacho, K. Holt, J. B. Kouri, J. T. Ramírez, M. J. Yacaman, *Nanotechnology*, **2005**, *16*, 2346.
69. S. Pal, Y. K. Tak, J. M. Song, *Appl. Environ. Microbiol.*, **2007**, *73*, 1712.

70. A. Desireddy, B. E. Conn, J. S. Guo, B. Yoon, R. N. Barnett, B. M. Monahan, K. Kirschbaum, W.P. Griffith, R. L. Whetten, U. Landman, T. P. Bigioni, *Nature*, **2013**, *501*, 399.

71. S. Eckhardt, P. S. Brunetto, J. Gagnon, M. Priebe, B. Giese, K. M. Fromm, *Chem. Rev.*, **2013**, *113*, 4708.

72. F. Wu, D. Liu, T. Wang, W. Li, X. Zhou, *J. Mater. Sci.: Mater. Electron.*, **2015**, *26*, 6781.

73. Z. S. Pillai, P. V. Kamat, *J. Phys. Chem. B*, **2004**, *108*, 945.

74. B. Khodashenas, H. R. Ghorbani, *Arabian J. Chem.,* in press. DOI:10.1016/j.arabjc.2014.12.014

75. C. Richmonds, R. M. Sankaran, *Appl. Phys. Lett.*, **2008**, *93*, 131501.

76. T. Parnklang, B. Lamlua, H. Gatemala, Ch. Thammacharoen, S. Kuimalee, B. Lohwongwatana, S. Ekgasit, *Mater. Chem. Phys.*, **2015**, *153*, 127.

77. Table of Characteristic IR Absorptions, available from: https://tecniquesinstrumentals.files.wordpress.com/2011/09/infrared-table-copia.pdf

78. S. Singh, A. Bharti, V. K. Meena, *J. Mater. Sci.: Mater. Electron.*, **2014**, *25*, 3747.

79. S. Agnihotri, S. Mukherji, S. Mukherji, *RSC Adv.*, **2014,** *4*, 3974.

4 Preparation of Au/Ag alloy nanoparticles in microwave induced plasma-in-liquid process (MWPLP)

4.1 Introduction

For several years now, bimetallic alloy nanoparticles (NPs) have attracted researchers from different fields, because of their unique electronic, optical, and catalytic properties,[1-7] combining properties of both metals or even bringing in new properties due to the synergy between the metals, which are superior to the

monometallic NPs.[8] Properties of these particles can be adjusted by changing their composition, size and structure (from random and mixed alloys to core-shell NPs). Tunability of the composition of alloy NPs is in high demand and interesting for variety of application.[9-11] This was successfully demonstrated for Au/Pd bimetallic NPs using microwave-induced plasma in liquid process (MWPLP).[12]

Intensive research has been undertaken for Au/Ag noble metal alloyed NPs due to their benefit to plasmonic applications, catalysis and biosensing.[13-18] However, a green synthesis of Au/Ag alloy NPs with mono-dispersed grain size and precise composition is still a great challenge.[19] Most of the current methods used for preparation of Au/Ag alloy NPs, i.e. chemical synthesis method,[20] phase-transfer,[21] digestive ripening[22] consists of time consuming complex multistep processes with high energy consumption, and therefore cost of the process and industrial application. Use of strong reducing and capping agents such as sodium borohydride ($NaBH_4$) and e.g., citrate,[23,24] respectively are necessary in this process and have, in fact impact on the environment. Use of several chemicals during the preparation of the NPs requires complicated and expensive purification process, which does not guarantee dispose of the impurities from the particles' surface or particles itself.

MWPLP is a new and green technique to produce pure metal NPs. The use of toxic reducing or capping agent can be avoided since metal ions are reduced by hydrogen radicals (H•) and solvated electrons (e^-_{aq}) generated by thermal decomposition of water molecules in the plasma process at reduced pressure. Monometallic NPs have been prepared in MWPLP, e.g. Au, Ag, Pt, etc.[25,26,28] However, it is challenging to synthesize bimetallic alloy using this method. Using

MWPLP, it was reported that bimetallic NPs of Au/Pd, Ag/Pt, Au/Pt, etc.[12,29,30] have been synthesized. However, the segregation of bimetal in single particles were observed and only a part of the obtained NPs was alloy.[12] Recently, Au/Ag alloy particles of ca. 11.0 nm were synthesized by Yan *et al.* in microplasma-chemical synthesis.[31] To the best of our knowledge, using the pure MWPLP, Au/Ag NPs have not been reported so far.

In this present research, we have used MWPLP as an alternative simple, green, energy and cost efficient method to synthesize Au/Ag alloy nanoparticles for the first time. The choice of metal precursors, *i.e.* $HAuCl_4$ and $[Ag(NH_3)_2]^+$ to be used at high pH, *i.e.* pH = 11, is crucial for co-reduction and alloying of Au and Ag in MWPLP. This condition allows for the homogeneous mixing of Au and Ag precursors and their similar reduction rates. Moreover, use of yttrium oxide (Y_2O_3) coated electrode in our system protects obtained particles from impurities caused by electrode materials in conventional plasma in liquid process.[25,26,27] We have investigated the formation process of the alloy NPs via monitoring of the reduction and NPs' growth and their composition changes during plasma discharge.

4.2 Aim of this chapter

I this chapter, Au/Ag alloy nanoparticles (NPs) were successfully prepared by one step synthesis using $HAuCl_4$ and $[Ag(NH_3)_2]^+$ as the precursors in microwave-induced plasma in liquid process (MWPLP) without addition of any organic protecting or reducing agents. The time dependent reduction and particle formation during 140 min plasma discharge were studied with TEM, UV-Vis spectra, ICP-OES. After 140 min, HAADF-STEM and EDX results directly

evidenced the formation of Au/Ag alloy NPs. Varying the input molar ratios of metal precursors allowed for control the composition of the Au/Ag alloy NPs.

4.3 Experimental section

4.3.1 Apparatus

The schematic illustration of plasma-in-liquid reactor and enlarged area with coated electrode are shown in Figure 4.1. Microwaves (2.45 GHz) are emitted from magnetron (Micro denshi UW-1500) and pass through a WRJ-2 rectangular waveguide (109.22 × 54.61 mm), a power meter, a tuner, a waveguide to the coaxial adaptor, and plasma source. The coaxial electrode is attached in the middle of waveguide and her front is projected in to the chamber. This coaxial electrode is ended by an Y_2O_3-coated stainless steel sharp tip (Figure 4.1). The stainless-steel reactor (500 cm^3) is coated inside with PTFE. Plasma solution is cooled by a stainless cooling spiral with chilled liquid at 5 °C. Plasma ignition and the solution during plasma reaction can be observed by eye through the quartz window. Pressure was decreased by a diaphragm vacuum pump and measured by a vacuum gauge.

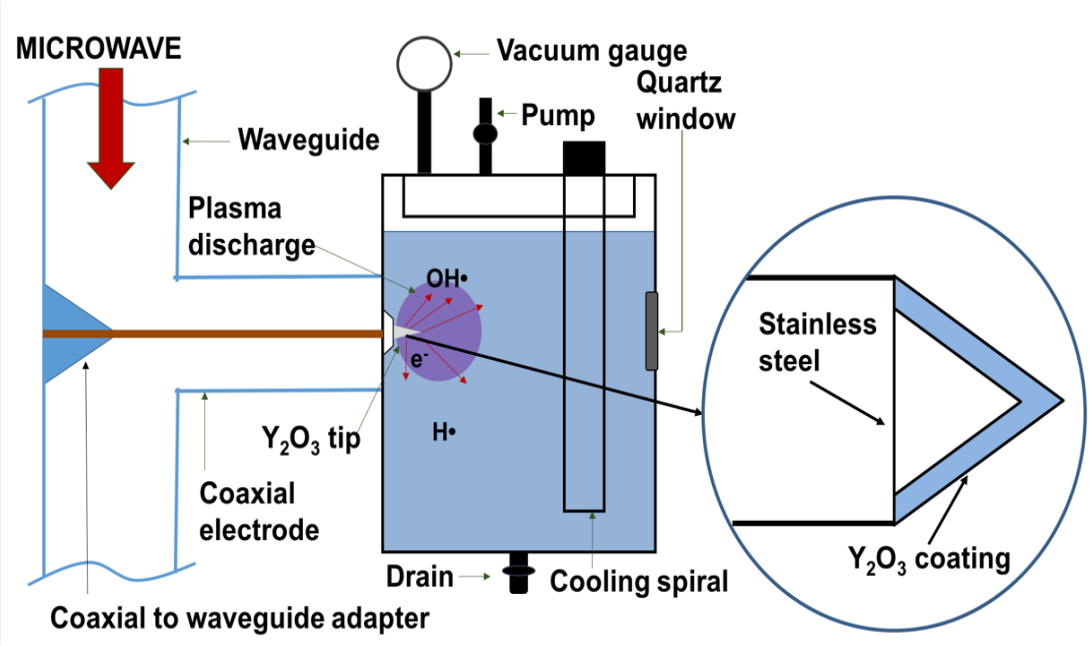

Figure 4.1 (a) Schematic illustration of the plasma reactor of microwave induced plasma-in-liquid process (MWPLP) used in this study and in enlarged area, configuration of the Y_2O_3-coated stainless steel electrode.

4.3.2 Materials

Silver nitrate ($AgNO_3$, min. 99.8%, Junsei, Japan) and Tetrachloroauric(III) acid hydrate ($HAuCl_4 \cdot nH_2O$ n=3.6, Kojima, Japan) were used as precursors. Ammonia (NH_3, min. 28%, GR, Junsei) was used for pH adjustment to pH 11.0 and for inductively coupled plasma optical emission spectrometry (ICP-OES). Nitric acid (HNO_3, min. 60%, Wako, Japan) and hydrochloric acid (HCl, min. 35%, Kanto Chemical, Japan) were used for preparation of samples for ICP-OES. All chemicals were used as received. The deionized water (Organo/ELGA purelabo system, > 18.2 MΩ·cm) was used to prepare solution for plasma reaction.

4.3.3 Synthesis of Au, Ag, and Au-Ag NPs

A typical synthesis of Au/Ag NPs with an input molar ratio Au:Ag = 2:2 (mol/mol) was conducted as follows. 2.12 cm^3 of aqueous $AgNO_3$ (0.12 M) was added into 250 cm^3 of water to obtain $AgNO_3$ concentration of 0.05 M in the final solution mix, the solution was stirred and ammonia solution (NH_4OH) was added to reach the desired pH level, pH 11.0. The same process was repeated for $HAuCl_4$, i.e. 5.02 cm^3 of aqueous $HAuCl_4$ (0.05 M) was added into 250 cm^3 of water to obtain $HAuCl_4$ concentration of 0.05 M in the final solution mix, the solution was stirred, and pH was adjusted to pH 11.0 by ammonia solution (NH_4OH). Both separately prepared solutions were mixed and stirred together for 10 minutes, and then introduced into the reaction vessel. The plasma was initiated at 500 W of the microwave output. Then, in order to keep plasma generation, the output was kept at 450 W during whole reaction. The plasma reaction was conducted for 140 min. As for the synthesis of pure Au, Ag, and Au/Ag alloy NPs with different composition, the amount of metal precursor solution was given in Table 4.1.

Table 4.1 Amount of used $HAuCl_4$ (0.05M) and $AgNO_3$ (0.12M) solutions for preparation of the 500 cm^3 mix precursor solutions for synthesis of Au, Ag, and Au/Ag NPs.

Experiment No.	0.05 M $HAuCl_4$ (cm^3)	0.12 M $AgNO_3$ (cm^3)	Au:Ag ratio (mol/mol)
1	10.04	0	4:0
2	7.53	1.06	3:1
3	5.02	2.12	2:2
4	2.51	3.18	1:3
5	0	4.24	0:4

4.3.4 Characterization

UV-Vis spectra were collected in order to observe Au/Ag NPs formation at different time and pH using an UV-Vis spectrophotometer (Shimadzu UV-1800) and a quartz cell with 10 mm optical path. During plasma reaction, 3 cm^3 of the sample solutions were taken directly from the plasma chamber for each measurement at various reaction time (20, 40, 100, 140 min).

The transmission electron microscopy (TEM, JEOL 2000FX, at 200 kV) with an energy dispersive X-ray spectroscope (EDX) was used to analyze the structure and sizes of Au-Ag bimetallic, Au and Ag NPs in time. Scanning transmission electron microscopy (STEM) observations and EDX mapping were carried out with a JEOL JEM-ARM-200F (200 kV) and a FEI Titan Cube (300 kV). NP dispersions were at first purified by membrane dialysis for 3 days, and then the purified solution was dropped on collodion film-coated copper TEM grids, and

naturally dried. Between 150 to 200 NPs were used to estimate the particle size, in arbitrary chosen areas, and size distribution using TEM images. A part of the NPs solutions was filtrated through 0.1 μm mixed cellulose filter and examined with X-ray diffraction (XRD, Rigaku MiniFlex II, Cu K*α* radiation, scanning rate of 5 ° min^{-1}). The inductively coupled plasma optical emission spectrometry (ICP-OES, ICPE-9000, Shimadzu) was used for observing the concentration of Au and Ag ions in time in the sample prepared using input ratio Au:Ag = 2:2 (mol/mol).

4.4 Result and discussion

During thermal decomposition of water in MWPLP, several reactive species such as hydrogen radicals, oxygen radicals, hydroxyl radicals as well as solvated electrons (e^-_{aq}) are generated. Hydrogen radicals and solvated electrons can act as a direct reducing species and reduce gold and silver ions/complex to Au^0, Ag^0, and Au^0/Ag^0 NPs as shown below (Eq. 1-3).

$$AuCl_{4-x}(OH)_x^- + 3e_{aq}^- \rightarrow Au^0 + (4-x)Cl^- + xOH^- \quad (1)$$

$$[Ag(NH_3)_2]^+ + e_{aq}^- + H_2O \rightarrow Ag^0 + 2NH_4^+ + 2OH^- \quad (2)$$

$$AuCl_{4-x}(OH)_x^- + [Ag(NH_3)_2]^+ + 4e_{aq}^- + H_2O \rightarrow Au^0Ag^0 + (4-x)Cl^- + (2+x)OH^- + 2NH_4^+ \quad (3)$$

XRD patterns

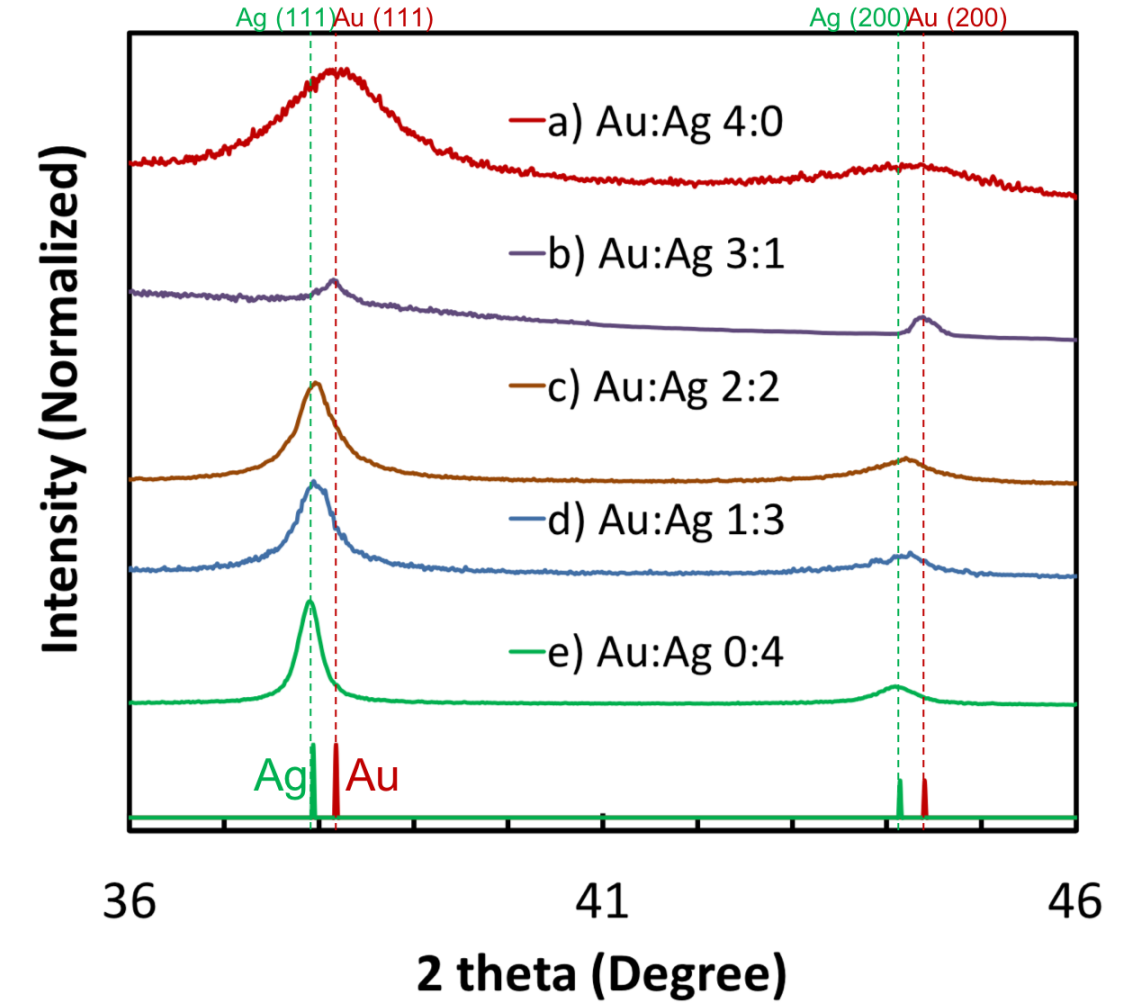

Figure 4.2 XRD patterns of NPs synthesized using different initial molar ratios Au:Ag = 4:0 (a), 3:1 (b), 2:2 (c), 1:3 (d), and 0:4 mol/mol (e). The dashed lines are for visual guide to mark position of (111) and (200) peaks for both Au and Ag. The reference patterns of Au (JCPDS no. 04-0784) and Ag (JCPDS no. 01-1164) are shown at the bottom.

XRD patterns of the obtained NPs prepared with different ratios of Au:Ag after 140 minutes of plasma reaction was shown in Figure 4.2. Peak positions of (111) and (200) planes for both Au and Ag are indicated in the figure by dashed line

and distinguished by color. Samples prepared using only Au precursor (Au:Ag = 4:0 (mol/mol)) and only Ag precursor (Au:Ag = 0:4 (mol/mol)) showed peaks for Au and Ag, respectively, in correspondence with standard references of Au and Ag. This indicated pure Au and Ag NPs were obtained. All the peaks in the XRD patterns (b)-(e) of Au/Ag NPs are relatively strong and lie between that of Au and Ag, indicated the formation of Au/Ag alloy NPs. Moreover, we were able to observe shifts in the peak positions from that of Ag to that of Au with an increase in the input ratio of Au from (e) to (b) (i.e. Au:Ag = 1:3 to 3:1 (mol/mol)). This can be caused by the increase in Au content in the obtained Au/Ag NPs.

4.4.1 UV-Vis spectra

When using only silver precursor (Au:Ag = 0:4 (mol/mol)), a broad surface plasmon resonance (SPR) absorption at 350-800 nm was observed in UV-Vis spectrum after 140 minutes of plasma irradiation (Figure 4.3). This was attributed to the big sized plate-like Ag NPs (show later in TEM image Figure 4.4e) as previously reported.[32,33] When only gold precursor was used, broad SPR peak was observed at 500-700 nm in the UV-Vis spectrum. On the other hand, using Au:Ag = 1:3, 2:2, and 3:1 (mol/mol) resulted to a single defined SPR peak around 450 nm. This can relate to the formation of Au/Ag alloy NPs, as reported elsewhere.[34,35] However, the UV-Vis peak position and shape depend on not only the alloying of Au and Ag but several factors such as particles' size, shape, and composition. Thus we investigated the morphology and composition of the obtained bimetallic samples to further confirm the Au/Ag alloy formation.

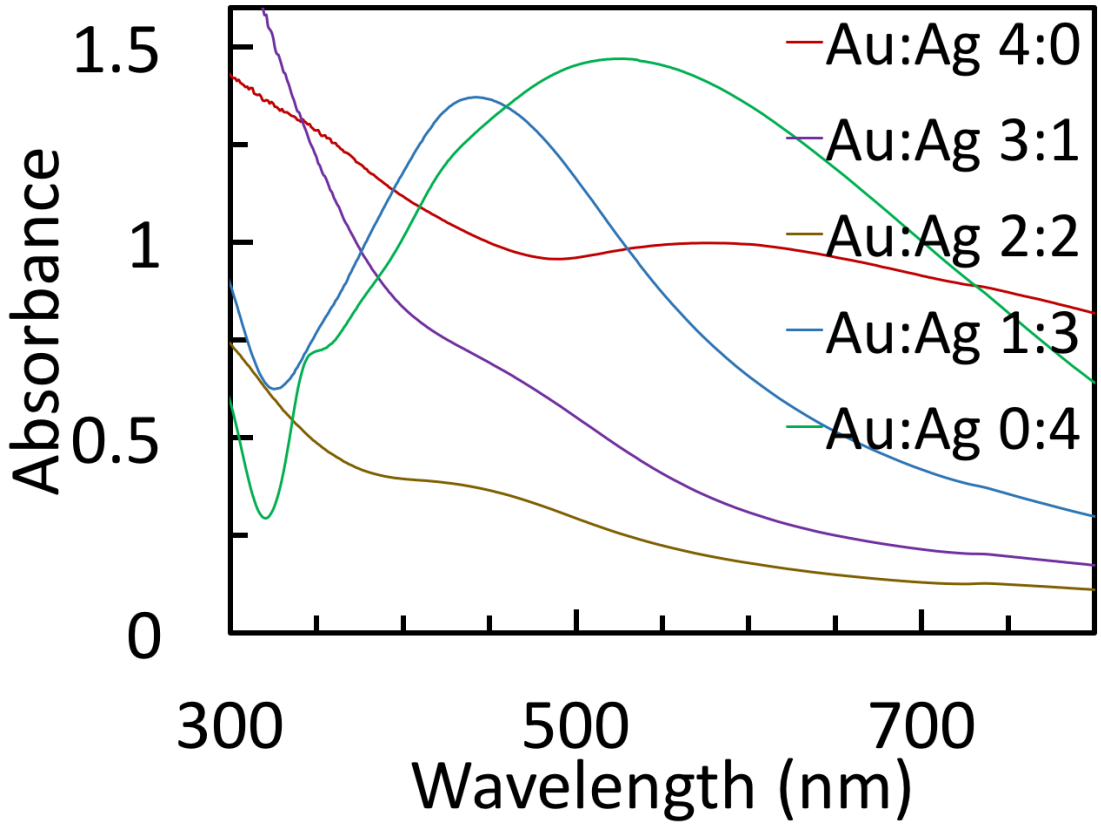

Figure 4.3 UV-Vis spectra for samples prepared with ratio Au:Ag = 4:0, 3:1, 1:3, 2:2, 0:4 (mol/mol) after 140 min of plasma discharge.

4.4.2 TEM images

Figure 4.4 shows TEM images of the synthesized Au, Au/Ag, and Ag NPs prepared using different input ratios, *i.e.*, Au:Ag = 4:0, 3:1, 2:2, 1:3, and 0:4 (mol/mol). Average diameters of these particles are shown in Table 4.2 and size distributions are given in Figure 4.5. The average diameter of monometallic plate-like Ag NPs, i.e. 128.8±18.9 nm, is significantly bigger than that of Au and Au/Ag NPs. When using Au:Ag = 4:0 and 3:1 mol/mol, NPs of 10 nm were obtained. Higher ratio of Ag used in synthesis (Au:Ag = 2:2, 1:3 (mol/mol)) resulted to Au/Ag

NPs with bimodal size distribution, i.e. small sized Au/Ag NPs of 3-5 nm and big sized Au/Ag NPs of 20-60 nm. This can relate to a complicated reduction, nucleation and growth process of Au/Ag NPs in MWPLP.

We notice that the spherical Ag NPs prepared in MWPLP showed an SPR peak at 420 nm in UV-Vis spectra,[33] and spherical Au NPs typically show an SPR peak between 500-600 nm.[36] Thus, the single SPR peaks observed around 450 nm (Figure 4.3) for Au/Ag NPs of 3-60 nm prepared using Au:Ag = 1:3, 2:2, and 3:1 (mol/mol) are more likely related to the formation of Au/Ag alloy, whereas the large size distribution of Au/Ag NPs may contribute to the broadening of the peak.

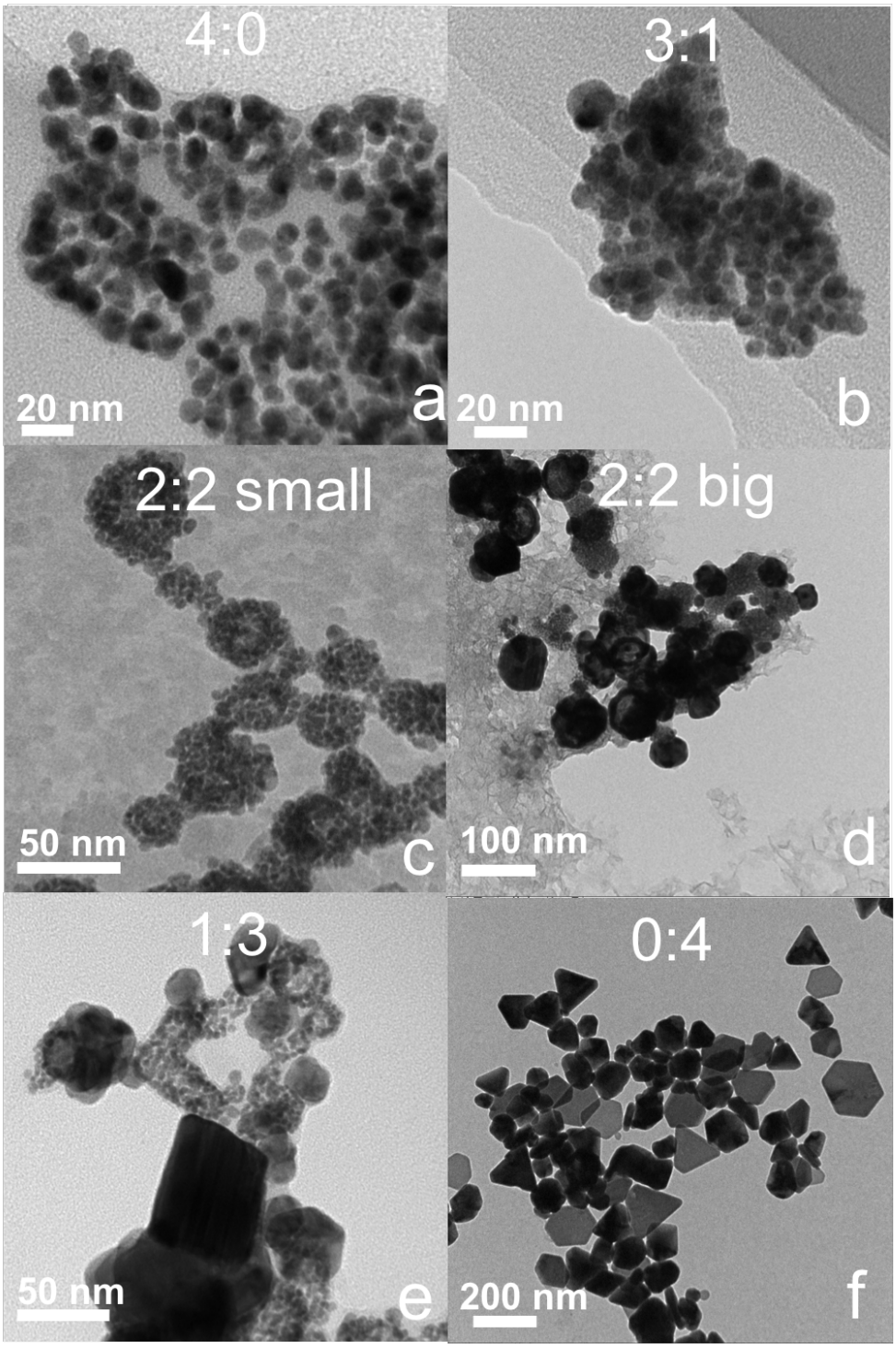

Figure 4.4 TEM images of Au, Ag and Au/Ag alloy NPs synthesized after 140 minutes of plasma reaction using different input molar ratio Au:Ag of a) 4:0, b) 3:1, c) and d) 2:2, e) 1:3, and f) 0:4.

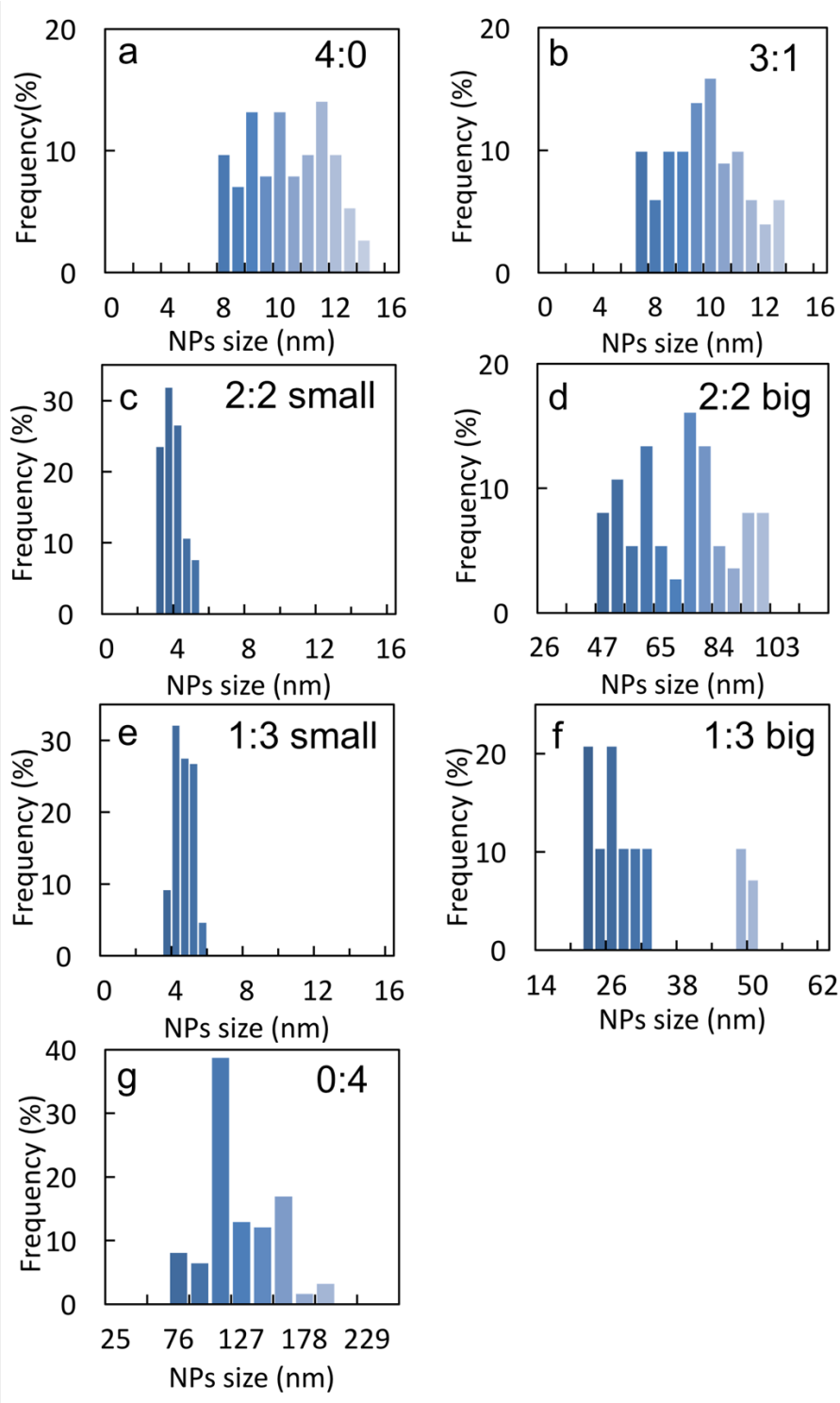

Figure 4.5 Particle size distribution for Au, Ag and AuAg alloy NPs synthesized after 140 minutes of plasma reaction using different molar ratio Au:Ag of a) 4:0, b) 3:1, c) 2:2 for small NPs d) 2:2 for big NPs, e) 1:3 for small NPs, f) 1:3 for big NPs, and e) 0:4.

Table 4.2 Average diameter of obtained NPs at different ratio Au:Ag (mol/mol) after 140 min of plasma discharge.

Au:Ag mol/mol	**4:0**	**3:1**	**2:2**	**1:3**	**0:4**
Small NPs (nm)	10.3±1.4	9.2±1.0	3.7±0.3	4.7±0.5	-
Big NPs (nm)	-	-	43.6±8.2	29.9±6.3	128.8±18.9

4.4.3 EDX mapping and Au/Ag alloy composition

HAADF-STEM and EDX mapping (Figures 4.6a-c) of several Au/Ag NPs (43.6 ± 4.7 nm), prepared using Au:Ag = 2:2 (mol/mol) confirmed the formation of Au/Ag alloy NPs. Elemental mapping of these particles showed homogeneous distribution of Au and Ag over the entire NP structure. Similar results were obtained for a single smaller Au/Ag NP of ca. 22.9 nm (Figures 4.6d-f). These results are consistent with XRD and UV-Vis results in formation of Au/Ag alloy NPs.

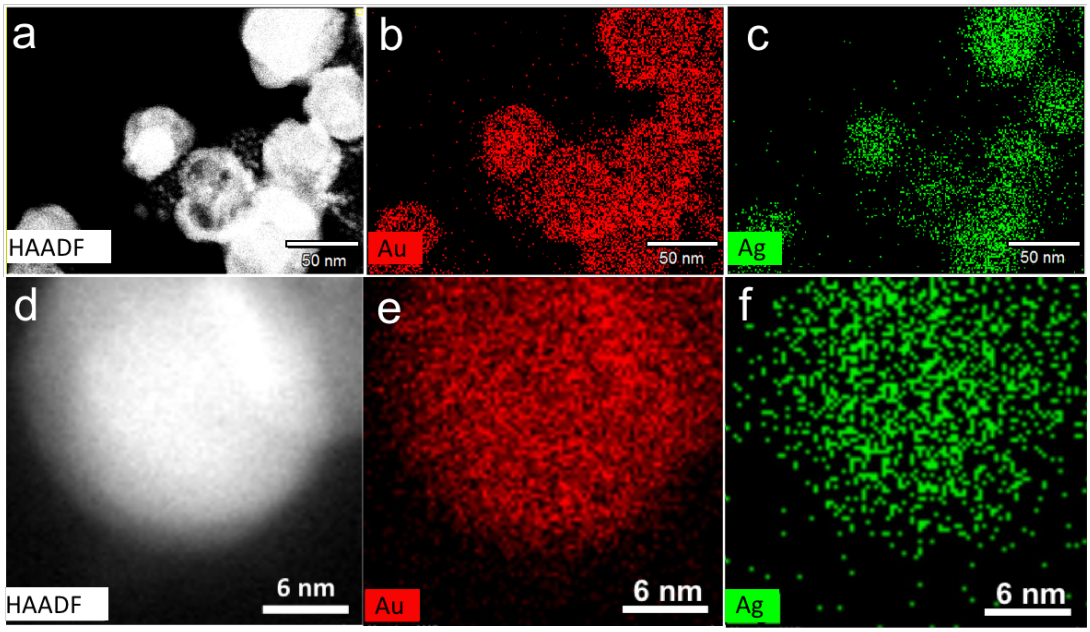

Figure 4.6 (a) HAADF image of several Au/Ag NPs prepared using input ratio Au:Ag = 2:2 (mol/mol) and EDX mapping images for (b) Au, (c) Ag; (c) HAADF, (d) and (e) EDX mappings images for Au and Ag of a single Au/Ag NP prepared using Au:Ag = 2:2 (mol/mol) input ratio.

EDX results (Table 4.3) showed relation between the elemental composition of the obtained NPs and the initial molar ratio of precursors used in the synthesis. Using Au:Ag = 1:3, 2:2, and 3:1 (mol/mol), i.e. 25, 50, and 75 mol% Au respectively, resulted to Au/Ag NPs composed of 26, 54, and 77 mol% of Au, respectively. The Au content in the obtained Au/Ag NPs can be well controlled via varying the initial molar ratios of metal precursors used. Calculations based on the lattice constants obtained from XRD (Figure 4.2) following Vegard's law, indicated alloy formation between gold and silver at nanometer scale (Table 4.3).

It was calculated that while using Au:Ag = 1:3, 2:2, and 3:1 (mol/mol), Au/Ag NPs were composed of 36, 40, and 89 mol % of Au, respectively.

Table 4.3. Composition of the obtained NPs synthesized using different initial Au:Ag molar ratios, measured by EDS and calculated from XRD by Vegard's law.

Input ratio		Au/Au NPs	
Au:Ag (mol/mol)	Au Content (mol%)	Au Content (mol%, EDS)	Au Content (mol%, XRD)
4:0	100	100	100
1:3	25	26	36
2:2	50	54	40
3:1	75	77	89
0:4	0	0	0

4.4.4 Discussion on particle formation

In order to understand the evolution of alloy NPs during plasma discharge, the UV-Vis spectra and composition of NPs at various reaction time were analyzed for equimolar Au/Ag NPs prepared with Au:Ag = 2:2 (mol/mol). The time dependent UV-Vis spectra indicated that there was no segregated Au and Ag SPR peaks during plasma discharge. This indicates the alloy form in every stage of the reaction. On the other hand, ICP-OES results (Figure 4.7) showed that in the first 60 min NPs composed of more than 75 at% of Au, then the content of Au decreased with reaction time and ended at 50 at% after 140 min plasma discharge. This may related to the easier reduction of Au compared with Ag in the MWPLP at pH=11.0. The detailed mechanism is unclear at this moment, but we think that the difference in the reduction of Au and Ag may influence the

particle size. As Au can be reduced mostly in early stage of plasma discharge and form nuclei for the growth of Au/Ag NPs. Thus, with more Au initial ratio used in the reaction solution, the number of nuclei increases and thus the obtained NPs become smaller. This tendency was consistent with particle size and size distribution of the obtained Au, Au/Ag, and Ag NPs.

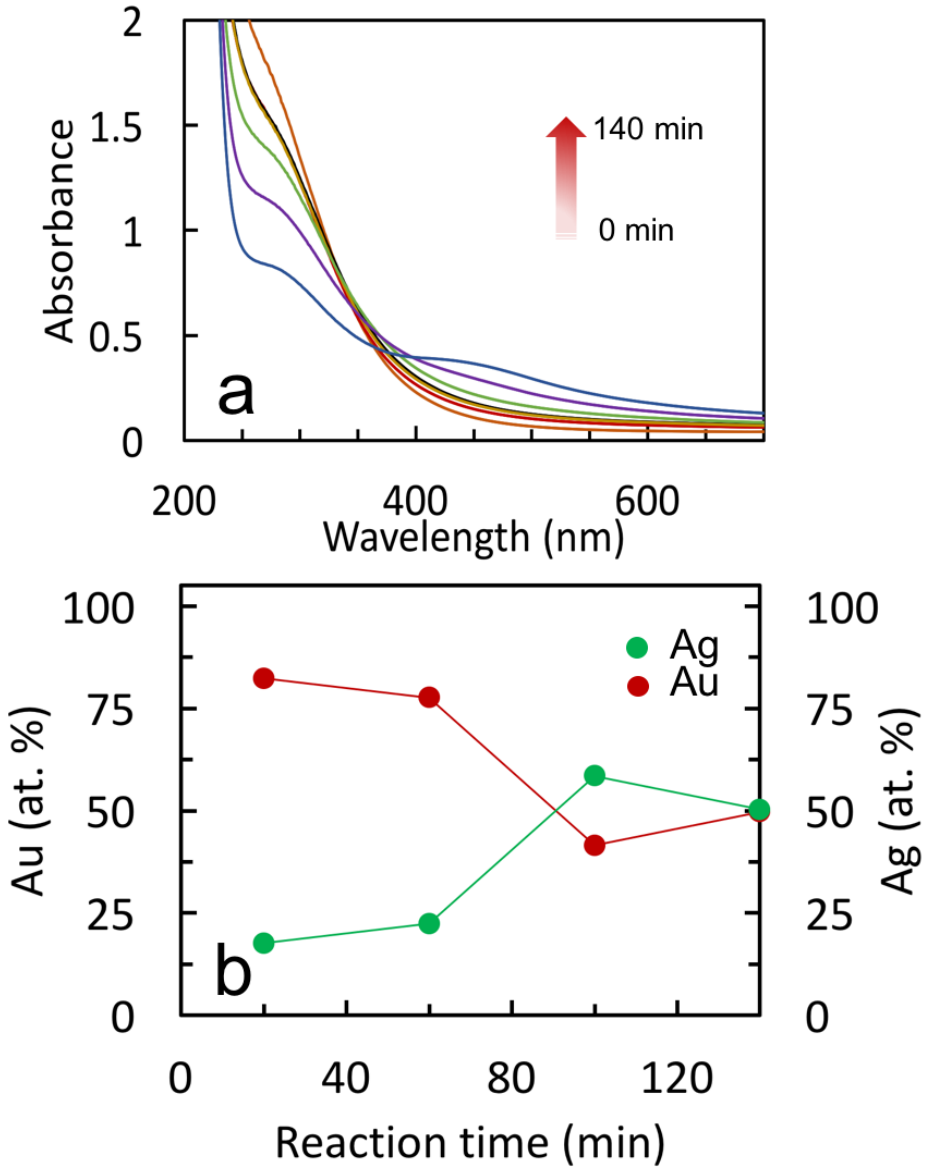

Figure 4.7 UV-Vis spectra (a) and composition measured by ICP-OES (b) for NPs prepared with input ratio Au:Ag = 2:2 (mol/mol) during 140 min plasma

discharge. The orange and blue dots denote for atomic contents (in percentage) of Au and Ag in Au/Ag NPs obtained during 140 min plasma discharge, respectively.

4.4.5 Colloidal stability of Au/Ag NP dispersions

Figure 4.8 shows photographs of the solutions after 140 minutes of plasma reaction for different initial ratio of Au:Ag. We can clearly see the difference in the solutions colour. Au/Ag alloy particles prepared at ratios 3:1, 2:2, and 1:3 have brownish color. None of the NP dispersions were precipitated after 140 min plasma discharge. It was observed negligible precipitation in the Au/Ag NPs for 4 days (Figure 4.8), indicating relatively good colloidal stability even though no surfactants or protecting agents were used.

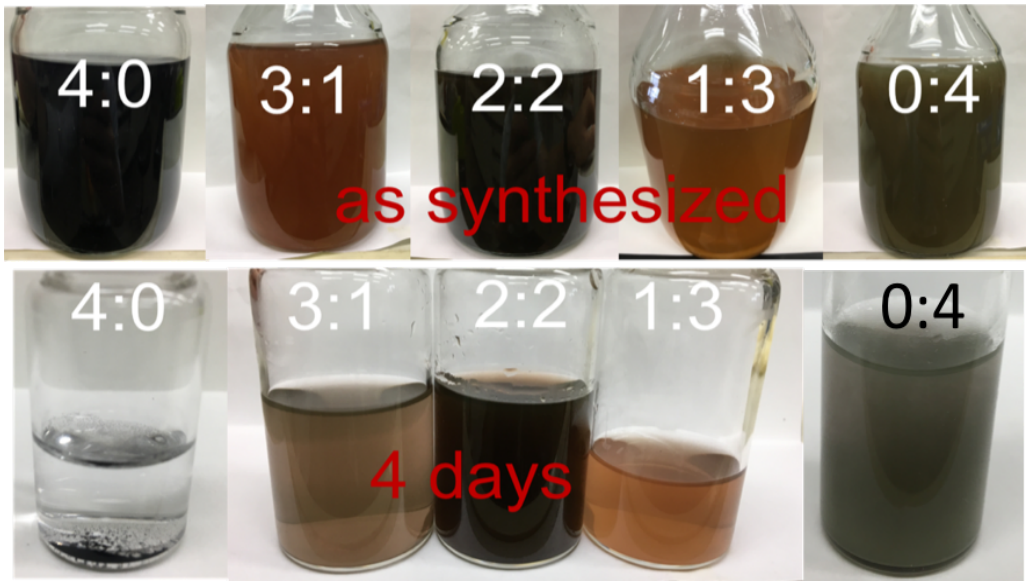

Figure 4.8 Photographs of the obtained dispersions (500 cm^3 bottles) after 140 minutes of plasma reaction with input molar ratios Au:Ag of (a) 4:0, (b) 3:1, (c)

2:2, (d) 1:3, (e) 0:4 (mol/mol). And stability of the NP dispersions (7 cm^3 bottles) prepared using Au:Ag of (f) 3:1, (g) 2:2, (h) 1:3 (mol/mol) after 4 days.

4.5 Conclusion

The last chapter of this thesis shows successful preparation of Au, Ag, and Au/Ag alloy NPs via reduction of molecular precursors by MWPLP without any protecting or reducing agent. The alloy NPs were confirmed with XRD, UV-Vis spectra, and by EDX mapping images. The composition of the Au/Ag NPs was controlled via varying the initial molar ratios of metal precursors. The results indicate that MWPLP with suitable choices of molecular precursors and reaction conditions can be used as a green method for creating alloy bimetallic NPs.

4.6 References

1 M. Broyer, E. Cottancin, J. Lerme, M. Pellarin, N.D. Fatti, F. Vallee, J. Burgin, C. Guillon, P. Langot, *Faraday Discuss.*, **2008**, *138*, 137.

2 X. F. Gu, T. Qiu, W. J. Zhang, P. K. Chu, *Nanoscale Res. Lett.*, **2011**, *6*, 199.

3 K.S. Lee, M. A. El-Sayed, *J. Phys. Chem. B.*, **2011**, *110*, 19220.

4 T. Mitsudome, Y. Mikami, H. Funai, T. Mizugaki, K. Jitsukawa, K. Kaneda, *Angew. Chem. Int. Ed.*, **2008**, *47*, 138.

5 C.-W. Yi, K. Luo, T. Wei, D. W. Goodman, *J. Phys. Chem. B*, **2005**, *109*, 18535.

6 M. T. Nguyen, T. Yonezawa, Y. Wang, T. Tokunaga, *Mater. Lett.*, **2016**, *171*, 75.

7 N. Toshima, T. Yonezawa, *New J. Chem.*, **1998**, *22*, 1179.

8 J.-H. Liu, A.-Q. Wang, Y.-S. Chi, H.-P. Lin, C.-Y. Mou, *J. Phys. Chem. B.*, **2005**, *109*, 40.

9 K. McNamara, S. A. M. Tofail, *Adv. Phys.: X.*, **2017,** *2*, 54.

10 M. Valenti, A. Venugopal, D. Tordera, M. P. Jonsson, G. Biskos, A. Schmidt-Ott, W. A. Smith, *ACS Photonics* **2017**, *4*, 1146.

11 T. Chen, V. O. Rodionov, *ACS Catal.*, **2016**, *6*, 4025.

12 H. Shirai, M. T. Nguyen, D. Čempel, H. Tsukamoto, T. Tokunaga, Y.-C. Liao, T. Yonezawa, *Bull. Chem. Soc. Jpn.*, **2017,** *90*, 279.

13 M. B. Cortie, X. Xu, M. J. Ford, *Phys. Chem. Chem. Phys.*, **2006**, *8*, 3520.

14 N. Harris, M. J. Ford, P. Mulvaney, M. B. Cortie, *Gold Bull.*, **2008**, *41*, 5.

15 J. Wilcoxon, *J. Phys. Chem. B*, 2009, *113*, 2647.

16 A.-Q. Wang, J.-H. Liu, S. D. Lin, T.-S. Lin, C.-Y. Mou, *J. Catal.*, **2005**, *233*, 186.

17 B. Xia, F. He, L. Li, *Langmuir*, **2013**, *29*, 4901.

18 X. Ren, X. Meng, F. Tang, *Sens. Actuator. B: Chem.*, **2005**, *110*, 358.

19 L. Sun, W. Luan, Y. J. Shan, *Nanoscale Res. Lett.*, **2012**, 7, 225.

20 A. Pal, S. Shah, S. Devi, *Colloid. Surf. A*, **2007**, *302*, 51.

21 M. J. Hostetler, C. J. Zhong, J. Anderegg, S. M. Gross, N. D. Evans, M. Porter, R. W. Murray, *J. Am. Chem. Soc.*, **1998**, *120*, 9396.

22 S. Link, Z. L. Wang, M. A. El-Sayed, *J. Phys. Chem. B.*, **1999**, *103*, 3529.

23 M. P. Mallin, C. J. Murphy, *Nano Lett.*, **2002**, *2*, 1235.

24 Q. Zhang, J.-Y. Lee, J. Yang, C. Boothroyd, J. Zhang, *Nanotechnology*, **2007**, *18*, 245605.

25 M. Nishimoto, T. Yonezawa, D. Čempel, M. T. Nguyen, Y. Ishida, H. Tsukamoto, *Mater. Chem. Phys.*, **2017**, *193*, 7.

26 D. Čempel, M. T. Nguyen, Y. Ishida, Y. Wang, K. C.-W. Wu, T. Yonezawa, *J. Nanosci. Nanotechnol.*, **2016**, 16, 9257.

27 Y. Ishida, Y. Motokane, T. Tokunaga, T. Yonezawa, *Phys. Chem. Chem. Phys.*, **2015**, 17, 24556.

28 S. Sato, K. Mori, O. Ariyada, H. Atsushi, T. Yonezawa, *Surf. Coat. Technol.*, **2011**, *206*, 955.

29 P. Pootawang, N. Saito, O. Takai, S.-Y. Lee, *Nanotechnology*, **2012**, *23*, 395602.

30 X. Hu, X. Shen, O. Takai, N. Saito, *J. Alloy. Compd.*, **2013**, *552*, 351.

31 T. Yan, X. Zhong, A. E. Rider, Y. Lu, S. A. Furman, K. Ostrikov, *Chem. Commun.*, **2014**, *50*, 3144.

32 M. Nishimoto, H. Tsukamoto, M. T. Nguyen, T. Yonezawa, *ChemistrySelect*, **2017**, *2*, 7873.

33 D. Čempel, M. T. Nguyen, Y. Ishida, T. Yonezawa, *Bull. Chem. Soc. Jpn.*, **2017,** doi:10.1246/bcsj.20170327.

34 A. K. Tiwari, S. Gangopadhyay, C.-H. Chang, S. Pande, S. K. Saha, *J. Colloid Interface Sci.*, **2015**, 445, 76.

35 K. Bagga, D. F. Brougham, T.E. Keyes, D. Brabazon, *Phys. Chem. Chem. Phys.*, **2015**,17, 27968.

36 X. Huang, M. A. El-Sayed, *J. Adv. Res.*, **2010**, 8, 13.

5 Concluding remarks

The second chapter of the thesis introduced ceramic (Y_2O_3)-coated electrode to the microwave-induced plasma in liquid process (MWPLP) to create highly pure Au NPs. L-arginine used as the protecting agent can stabilize NPs from severe aggregation in the whole studied pH range (3.5-12.0) via adsorption on

Au NP's surface and creation of a layer for repulsive interaction between NPs. The bimodal size distribution of Au NPs was observed for pH in range of 3.5 – 12.0. Small sized (average size 2.1 – 3.1 nm) Au NPs were dominant at pH 6.0 and 12.0 while large sized ones were considerable at pH = 3.5. Study of Au^{3+} ions reduction rate showed that the reduction is rapid in the first 20 minutes of the reaction and then decrease with prolonging plasma discharge time. About 89% of Au complexes were reduced for pH 12.0 after 140 minutes of the plasma reaction, and more than 99% of the Au complexes for pH 3.5 and 6.0. A low reduction rate of Au^{3+} ions (different from citrate reduction and plasma in liquid method using uncoated electrode, where the reduction is completed within a minute) and non-homogenous NP growth can be taken into account for the bimodal size distribution obtained using coated electrode in MWPLP. As a result, different from the case of PLP by pulse discharge with uncoated electrodes, a strong dependence between pH and particle size was not observed in our case, instead a redistribution of the number of big and small NPs was varied with pH. The synthesized Au NPs exhibited high purity without any contamination from the electrode materials.

The third chapter shows the influence of silver diamine complex as the precursor and L-arginine as a stabilizing agent on the formation of Ag NPs synthesized in MWPLP using a coated electrode. Using silver nitrate as the precursor for synthesis of Ag NPs had similar effect on the formation of the NPs as in case of Au NPs investigated in chapter 2, the obtained particles showed bimodal size distribution with small NPs about 8.3 nm and big NPs with size about 88.4 nm. Change of initial precursor from silver nitrate to silver diamine complex

increased reduction speed of Ag^+ ions and therefore improved size distribution of the obtained NPs. The obtained NPs were about 128.7 nm in diameter and showed plate-like structure of the NPs. The addition of the L-arginine at the certain ratio of silver diamine complex to L-arginine (higher than 1:2 ratio) decreased the size of the NPs significantly to the particles with average diameter of ca. 5nm. As a result, a strong influence of L-arginine on NP size, and of silver diamine complex on the uniformity of the synthesized Ag NPs was observed. In conclusion, uniform, small sized and highly pure Ag NPs can be obtained by addition of silver diamine and L-arginine during MWPLP. The obtained Ag NPs were effectively stabilized by carboxylate group contributed by L-arginine as was confirmed by FT-IR.

The last experimental chapter of the thesis shows successful preparation of Au, Ag, and Au/Ag alloy NPs via reduction of molecular precursors by MWPLP without any protecting or reducing agent. By varying the initial molar ratios of metal precursors it's possible to control the composition of the Au/Ag NPs. This was proved by observation of the shift of XRD peaks' positions with the change of initial molar ratio of metal precursors. ICP-OES for the NPs prepared with the initial ratio of precursors Au:Ag=2:2 suggested that after 140 min NPs were formed by 50% of Au and 50% of Ag. STEM-EDS confirmed homogeneous distribution of Au and Ag over particles for the sample prepared with initial ratio of precursors Au:Ag=2:2. The alloy NPs were confirmed with XRD, UV-Vis spectra, and by EDX mapping images. The results indicate that MWPLP with suitable choices of molecular precursors and reaction conditions can be used as a green method for creating alloy bimetallic NPs.

Studies related to this thesis bring a better understanding and new look on the monometallic nanoparticles preparation in liquid plasma process as well as new approach for synthesis of bimetallic nanoparticles. Highly pure monometallic nanoparticles with controlled size and uniformity as well as bimetallic nanoparticles with tunable composition were prepared in this green method. Use of coated electrode brings a new option to preserve particles from contamination emitted by electrode materials. Better understanding of the mechanism of nanoparticles formation may open space to the more efficient industrial use of plasma in liquid process.

6 List of publications

1. **D. Čempel**, M. T. Nguyen, Y. Ishida, Y. Wang, K. C.-W. Wu, T. Yonezawa, Au nanoparticles prepared using a coated electrode in plasma-in-liquid process: Effect of the solution pH, *Journal of Nanoscience and Nanotechnology* 16 (2016); 9257-92622.

2. **D. Čempel**, M. T. Nguyen, T. Yonezawa, and Y. Ishida, L-arginine Stabilized Highly Uniform Ag Nanoparticles Prepared in Microwave Induced Plasma-in-Liquid Process (MWPLP), *Bull. Chem. Soc. Jpn.*, **2018,** doi:10.1246/bcsj.20170327

3. **D. Čempel**, M. T. Nguyen, Y. Ishida, T. Tokunaga, T. Yonezawa, Ligand Free Green Plasma-in-Liquid Synthesis of Au/Ag Alloy Nanoparticles, *New J. Chem*, **2018**, **Submitted paper.**

Related publications

4. H. Shirai, M. T. Nguyen, **D. Čempel**, H. Tsukamoto, T. Tokunaga, Y.-C. Liao, T. Yonezawa, Preparation of Au/Pd Bimetallic Nanoparticles by a Microwave-Induced Plasma in Liquid Process, *Bull. Chem. Soc. Jpn.* 90 (2017), 279-285, doi:10.1246/bcsj.20160333

5. M. Nishimoto, T. Yonezawa, **D. Čempel**, M. T. Nguyen, Y. Ishida, H. Tsukamoto, Effect of H_2O_2 on Au nanoparticle preparation using microwave-induced plasma in liquid, *Materials Chemistry and Physics* 193 (2017) 7-12, doi: 10.1016/j.matchemphys.2017.02.009